7 Quality Control and Assurance Procedures

7.1 Quality Implementation

An important aspect of the plasma spray technique is the development and implementation of stringent quality control and assurance procedures to ensure consistency in the properties of the coatings. Because a multitude of spray parameters can potentially influence the coating properties, parameter optimization involves statistical experimental design procedures. Such procedures provide a maximum of information on the behavior of a system with a minimum number of experiments. Thus there is generally a very favorable experimental economy that can save time and resources, and hence money. Principles of multifactorial analyses and several case studies will be dealt with in Chapter 8.

7.1.1 Total Quality Management

Total quality management, TQM, is a complex system of several innovative and interacting disciplines including management ('Achieving success through others'), philosophy, psychology, stochastics, engineering and scientific expertise. It involves the concept of continuous improvement (Japanese: Keizen), and can be divided into three groups and classified as *quality tools*, *quality philosophy*, and *management style*. To successfully implement TQM it is mandatory that all three units are linked, and interact smoothly. It is generally not sufficient to improve only one or two of these pillars of TQM. Even though some advantages will be gained the final product will not be optimized. Thus TQM is more than just a 'quality' evolution but a system of continuous improvement of the process and the product. The impressive success of Japanese industry in the past decades had its roots in rigorous TQM procedures [1, 2].

7.1.1.1 Quality Tools

Statistical design of experiments (SDE) is the backbone 'quality tool' of TQM. Using SDE many of the factors can be screened out that vitally control the process

and/or the product performance. Closely associated with SDE is statistical experimental strategy (SES) that attempts to answer crucially important questions at the start of a research program such as the number of experiments needed, the number and ranges of the parameters to be selected, the costs of the program, the equipment and manpower needed, the duration[1] etc. Likewise important is the initial selection of the quality characteristics that the experimental program is supposed to satisfy, i.e. the customer expectation. This will allow confident declaration of what, exactly, the analyses of the experimental data will teach the experimenter about the system under investigation. Linking SDE with SES will establish the only way to plan and execute experiments at conditions that will result in valid and statistically accurate and precise conclusions.

Several other quality tools also mostly based on statistics join in. These are statistical quality assurance (SQA) [3], statistical quality control (SQC) [4], Pareto and other distributions [5], cause–effect diagrams, benchmarking [6], the just-in-time (JIT) concept [7] and more. The most widely applied methods are *statistical process control* (SPC) [8] and *quality function deployment* (QFD) [9].

After factor screening by SDE/SES and determination of those factors that significantly influence the plasma spraying process and the coating properties, statistical process control is used to control the process so that despite the existence of internal and external variations the deposited coating is always within design specification. However, if information about the ranking of the controlling factors, i.e. their importance, is lacking the experimenter risks assuming that he/she is in control of a good process with SPC when in reality a nonoptimized process is being controlled (i.e. a local instead of a global extremum of the response surface), or worse, nonimportant factors [10].

An important element of TQM is quality function deployment. The customer of the deposited coating defines its 'quality', i.e. a set of properties that must be adhered to. This information supplied by the customer is analysed by the research team and transformed into engineering design and specification requirements. If this is done properly the final coating will have the predefined 'quality' even if the customer as a nonexpert cannot explain this desired 'quality' in engineering terms.

7.1.1.2 Quality Philosophy

With QFD entering the picture the dichotomy between nonexpert customer and expert designer/engineer can be resolved. In general, the two sources of quality are the research/engineering/technical staff of the coating developer, and the customers that define the term 'quality of the coating'. Since the most important asset of any organization is its staff, empowerment of that staff will be a natural part of any TQM implementation. This means that as much information about the process and the product must flow up and down the hierarchical structures of the company as needed

[1] This is not a trivial task. Starting a research program is rather easy but it takes guts and confidence to stop a program if it does not yield the desired results, i.e. if the program is not on time and within the allocated budget. Managers be aware: 'Self-perpetuating' programs usually waste resources and block the execution of other potentially more promising projects!

by the staff to understand the customers' needs. This informational empowerment encourages staff participation at all levels of the organization with the result of the creation of a considerable degree of initiative, commitment and motivation: a static and routine custodial organization is being transformed to a dynamic and flexible intra- and entrepreneurial one [10]. Because the process and the product quality requirements are fully understood by staff, it will be possible to anticipate, conform to, and also exceed the customers requirements. Only then 'total quality' can be achieved: doing the right things right, the first time, any time!

7.1.1.3 Management Style

The quality philosophy expounded above can only succeed if the style of management matches the quality philosophy's quest for motivation and challenge. This means that no philosophy can work unless it is applied, and it cannot be applied unless it is encouraged [10]. Products not conforming to quality are being subjected to a detailed 'failure/success analysis' or 'design/process monitoring'. The result of such types of analyses is to decide what needs to be done so that the root causes of the unreliability can be controlled. This is the hallmark of a successful TQM: to control the process, not the staff. Staff will feel encouraged to strive for continuous improvement that will create a high degree of autonomy of the teams and an increased level of responsiveness. While working under such conditions of 'enlightened participatory management' team members build trust and respect, share vital information and acquire common values. Hence a code of conduct is created that helps to resolve conflicts effectively and rapidly. In the end productivity as well as quality will be maximized. Several theories describe the productivity improvement operations such as 'Theory Z' [11], Juran's Quality Trilogy [12], Deming's Principles [13] and Crosby's 14 Steps [14].

To conclude the TQM approach involves a chain of events that should be implemented in order to arrive at a high quality process that will result in a high quality product, in this case a superior plasma-sprayed coating that meets the customers demand and expectations. The quality tools of this chain link research, development and product: SDE/SES identify those plasma spray parameters that significantly influence coating performance, process-based SPC ensures consistency in the industrial production of coating through Taguchi-type control designs, and QFD translates consumer demands into technical reality, i.e. engineering factors.

An excellent example how to introduce a quality management system based on the ISO 9001 [15] into a thermal spray company was recently given by Ebert and Verpoort [16]. The ISO 9001 standard is a model for quality assurance in design and development, production and servicing. It contains 20 quality management elements that were described in detail for a company developing new coatings and application areas.

7.1.2 Qualification Procedures

Qualification procedures of equipment, spray powders, process design and implementation, and operators are a mandatory part of TQM.

The success of plasma-sprayed coatings depends on the skill of the operator, the condition of the equipment, and the selection and optimization of the internal and external process variables. Thus it is logical that qualification tests be part of any quality assurance and TQM programs implemented by an organization required to produce components for severe service. The major purchasers of plasma-sprayed components for aircraft engines, for example, require potential suppliers to demonstrate their capabilities before being approved as vendors. The qualification procedures are intended to establish that the vendor has operators, equipment, and processes capable of producing plasma-spayed coatings of acceptable quality and service life.

As far as plasma-spray system operators are concerned, qualification procedures should demonstrate skill and knowledge, the ability to follow process instructions, and eventually to produce acceptable products. As in the widely used welding qualification procedures, a combination of the following excercises is deemed appropriate [17].

- The operator should take and pass a short written test covering questions pertinent to cleaning, surface preparation and masking procedures, and the general principles of the plasma-spraying equipment and procedures.
- The operator should demonstrate familiarity with appropriate equipment by connecting, setting up, and operating plasma-arc spraying equipment safely according to manuals supplied by the manufacturers.
- The operator should demonstrate capability by depositing an acceptable coating to a specified thickness on an appropriate test specimen. The quality of the test coating should be judged by suitable methods such as bond strength.

The qualification of plasma-spray equipment required by purchasers of critical components is usually directed towards two quality control objectives. First, using a qualified operator, the equipment must be shown to be capable of producing coatings that meet the acceptance quality agreed upon by the vendor and the purchaser. Second, all of the control and metering devices governing deposition variables must be shown to be properly calibrated and checked at regular intervals but at least every 30 days [17].

The purchaser of high quality plasma-spray coated parts normally requires that the deposition process proposed for production be qualified by experiments, in general using methods and principles of SDE. In the qualification tests, the coatings are deposited on strips or samples of standard size representing the material and surface characteristics of those to be used in the spray shop. The coatings are deposited to a specified thickness by qualified operators using written process sheets and qualified, calibrated equipment. Then the coatings will be evaluated by test methods mutually agreed upon.

7.1.3 Powder Characterization

The suppliers of spray powders, and shot and grit used to roughen the surface of the parts to be coated normally provide chemical analyses and information about the particle size of the material. When chemical compositions are to be checked, standard analytical methods are employed. When analyzing metals optical emission

spectroscopy, X-ray fluorescence spectroscopy or ICP spectrometry will be used. Gas contents such as oxygen and nitrogen of metal powders, coatings and substrates are determined by vacuum fusion.

The particle size distribution of spray powders can be determined by a variety of methods and described by different designations. For particle sizes larger than 45 μm the range is characterized by the minimum and maximum cumulative percentages, by mass, that will pass through or be retained by sieves with different designations (ISO designation: mm and μm, respectively; ASTM designation: mesh size). In general, sieving is done with a set of standard sieves, for example ASTM E11-70 [18] and B214-66 [19], assembled in suitable order by nesting in a mechanical shaker. The mass of powder retained at the appropriate sieves is weighed with a balance to a sensitivity of 0.01 g. The recommended sample masses for sieve analyses are 100 g and 50 g for materials having apparent densities, respectively, above or below 1 500 $Mg\,m^{-3}$. Data obtained from a sieve analysis of a plasma-spray powder should identify the specific mass fractions passing a particular size opening and retained on screens with smaller openings. The classification should be in size steps small enough to be useful for characterizing the material.

Particle sizes smaller than 45 μm are used to produce coatings with a very smooth finish. Their size distributions are normally determined by the elutriation method described in ASTM specification D293-60 [20]. The method is based on the velocity of particles falling in a countercurrent of air or gas. The results are not strictly accurate for porous particles. Better accuracies can be obtained by applying the Coulter Counter that measures the change in electrical resistivity across an orifice as particles suspended in a electrolyte are passed through the orifice. This change in resistivity is related to the volume of the particles. The effective size range of this instrument is 1.0 to 500 μm. Sedimentation techniques, for example the MSA (Mining Safety Appliance) apparatus extend the particle range to be measured to the submicron range (0.1–80 μm). Modern laser-operated particle analyzers allow for an automated measuring protocol.

'True' particle and coating densities can be determined by Archimedes' technique by dividing the mass of the sample by the volume of water it displaces. If the powder is representative of the material in the coating after plasma spraying, the density determination can be used to compute the porosity of the sprayed coating. More exact densities can be obtained with a helium–air pycnometer.

Useful information on flow rates and apparent densities of powders can be obtained with the Hall Flow Funnel. Data give information on the ease of handling of the powder during processing as well as the densities to expect when powder is placed in the powder feeding device.

7.2 Characterization and Test Procedures

To test and qualify coatings, a limited set of procedures are applied to evaluate *mechanical* (cohesive and adhesive bond strength, shear strength, macro- and microhardness, fracture toughness), *tribological* (wear, mechanical fatigue) and *chemical* (corrosion, oxidation) properties.

7.2.1 Mechanical Properties

7.2.1.1 Bond Strength

The quality of a thermally sprayed coating is, to a large extent, determined by the quality of its adhesion to the substrate. While it is generally assumed that the main contribution to the adhesion is a mechanical interlocking of the particle splats with asperities of the grit-blasted substrate surface, increasingly chemisorptive and epitaxial processes are considered important contributors to coating adhesion [21]. This assumption is partly based on the experimental evidence that the presence of intermediate bond coats, preheating of the substrate and high particle temperatures generated by increased plasma enthalpy and/or the residence time translate into thermally activated bonding mechanisms.

Recent results by Gawne *et al.* [22a] indicate that mechanical interlocking may only play a secondary role in coating adhesion. Surface roughening by grit-blasting is then considered only a vehicle to promote disc-shaped particle splats and consequently to suppress exploded splash-type splats. The latter result in voids at the coating–substrate interface because the spaces between individual splashes may be too small for the second lamella to penetrate. Secondly, the flattening on impact of the splash-type splats is more extensive than for the disc-shaped splats. Consequently the lamellae are thinner, cool more rapidly and thus decrease the time available for chemical bonding. Thirdly, during splashing the particles break up into smaller droplets resulting in a loss of continuity of the flowing melt and thus decreased bonding to the substrate.

The requirement of a roughened substrate surface can apparently be relaxed by the application of an initial thin layer (about 25 μm) of ceramic on a smooth metal surface by low-pressure plasma spraying (LPPS) followed by the application of a thermal barrier coating (TBC) by APS technique [22b]. The smooth surface can be an uncoated oxidation-resistant alloy, a metallic diffusion coating, or a plasma-sprayed metallic bond coat ground smooth or even lapped. The LPPS ceramic layer adheres well to the smooth metallic surface but its top surface is sufficiently rough to accommodate the normal thick TBC.

Over the years a large variety of different tests have been devised to measure bond strengths in an accurate and reproducible way. Despite those efforts, however, there is, to date, no reliable method available that can be generally applied to any kind of coating on any kind of substrate. An older review by Davies and Whittaker [23] identified the ultracentrifuge and various ultrasonic techniques as those that could presumably successfully meet the requirements of routine quality control. However, the tensile pull test is still most widely used to determine bond strength [24] even though there is a rather urgent call to interprete tensile adhesion tests in terms of a more appropriate design philosophy [25].

Tensile tests with adhesive

The strength of the bond between a plasma-sprayed coating and the substrate is extremely important for most coating applications. For this reason, tensile testing is most commonly applied to evaluate the cohesive and/or adhesive strength as de-

scribed by the ASTM Specification C633-79 [26] or DIN 50 160 [27]. The main differences between these tests concern the sample dimensions. The method is limited to rather thick coatings exceeding 380 μm (ASTM C633-79) and 150 μm (DIN 50 160), respectively.

As pointed out by Milewski [28] the tensile test methods can be subdivided into, first, tests in which the coatings are pulled off from the substrate with the help of a counter-fixture glued or soldered to the coating, and, second, tests in which the coatings are pulled off from an appropriately formed auxilliary fixture without an adhesive (Sharivker/Ollard test, see below).

Because of the properties of the organic adhesives used application of the test is at or near room temperature. The method is recommended for qualification, quality control, and component or process acceptance testing. It also is applied frequently to compare the adhesive or cohesive strengths of different coatings or different methods of substrate preparation. However, because of complicating factors such as the penetration of the adhesive into a porous coating, the strength data obtained are not suitable for design purposes. Figure 7-1 shows the fixtures for aligning the test specimens [26]. A test specimen consists of a substrate fixture to which the sprayed coating is applied, and a loading fixture. Both fixtures should be round solid cylinders not substantially shorter than their diameters that should be between 23 and 25 mm. The fixtures should be preferably made from the same material that will be used for the production substrates. The material used for adhesive bonding the loading fixture to the substrate fixture must have a tensile strength at least as high as the adhesive and cohesive strengths of the coating. The adhesive should be sufficiently viscous not to penetrate through the coating.

The bonding strength or the cohesive strength of the coating is determined by the quotient of the maximum load F in N required to separate the two fixtures subjected to the tensile test, and the cross-sectional area A in mm^2: Strength $= F/A$ [$N\,mm^{-2}$]. If the failure occurs entirely at the coating–substrate interface, the value is reported as *adhesion strength*. If the failure occurs entirely in the coating, the measured strength is considered the *cohesive strength* of the coating. Failure in the adhesive can be considered a satisfactory result if the strength value exceeds requirements for quality assurance or qualification tests (Fig. 7-2).

This qualitative distinction between adhesive and cohesive failure modes of a coating can be quantified by a modified ASTM C633-79 tensile test jig developed by Berndt [29] that is able to measure the extension of the specimen during loading. Since already slight misalignments of the specimen with respect to the pulling axis cause inappropriate errors in determining the failure load, any deviations were taken into account by using clip gages positioned on opposite sides of the jig. For tensile experiments using this modified test set-up on ZrO_2–8wt% Y_2O_3–NiCrAlY 'tandem' coatings it was found that the stress/strain data approximately fitted a straight line, i.e. the slope of the stress/strain plot is directly proportional to Young's modulus. The probability plot of the stress/strain gradients (Fig. 7-3) reveals a bimodal distribution: large gradients, i.e. large moduli correspond to adhesive failure, small gradients, i.e. low moduli correspond to cohesive failure. Mixed-mode failures are distributed over the entire gradient range.

The German specification DIN 50 160/10.90, analogous to ASTM C633, has been

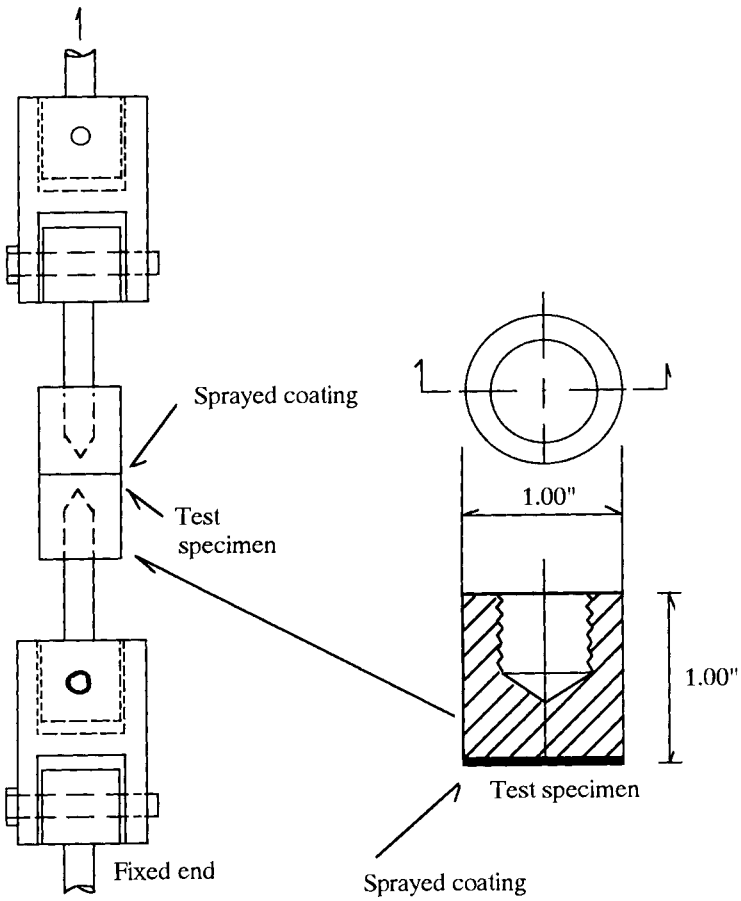

Figure 7-1. Loading fixture used to align the test specimens according to ASTM Designation C633-79 [26].

recently replaced by the European Standard EN 582:1993 [107]. This specification prescribes loading and coated substrate fixtures (configuration A) that allow for torsion- and momentum-free fixation by using ball- and socket-joints. Also, there is provision for having a coated disk of 25 or 40 mm diameter glued between two loading fixtures (configuration B).

Tensile tests without adhesive

Tensile tests without using an adhesive avoid the problem of the adhesive penetrating into open porosity of the coatings thus compromizing the accuracy of the measurement. Also, interpretative problems related to the influence of the coating thickness on the measured strength values could presumably be alleviated. The Ollard–Sharivker test [30, 31] uses a special jig (Fig. 7-4a) consisting of a base and a smoothly fitting washer supported on the shoulder of the base. This device is grit-

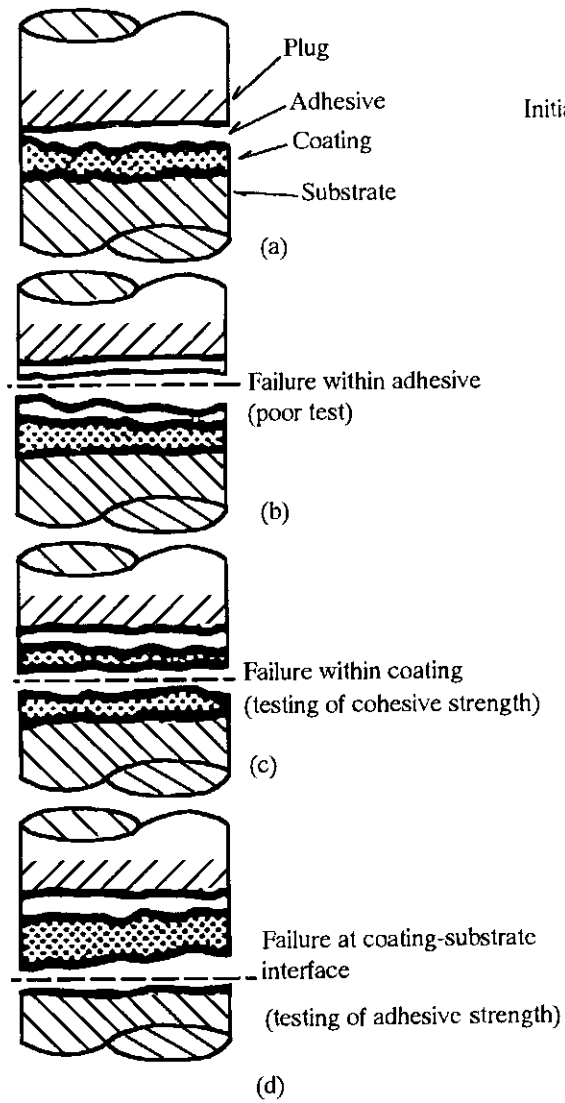

Figure 7-2. Failure surfaces of loading and substrate fixtures.

blasted and inserted into a plasma spray apparatus through which the top face is coated as shown in the figure. The adhesion strength is determined by tearing away the base from the coating. Since the adhesion strength appears to be a function of the coating thickness, it seems feasible to determine the value of adhesion strength unaffected by internal stresses by extrapolating the adhesion strength vs. coating thickness curve to zero thickness as shown in Fig. 7-4b. When a certain critical coating thickness, δ_c, is reached, spontaneous peeling of the coating from the substrate is observed. With decreasing thickness the strength of adhesion increases linearly. Failure takes place in an adhesion-type stripping mode along the coating/substrate

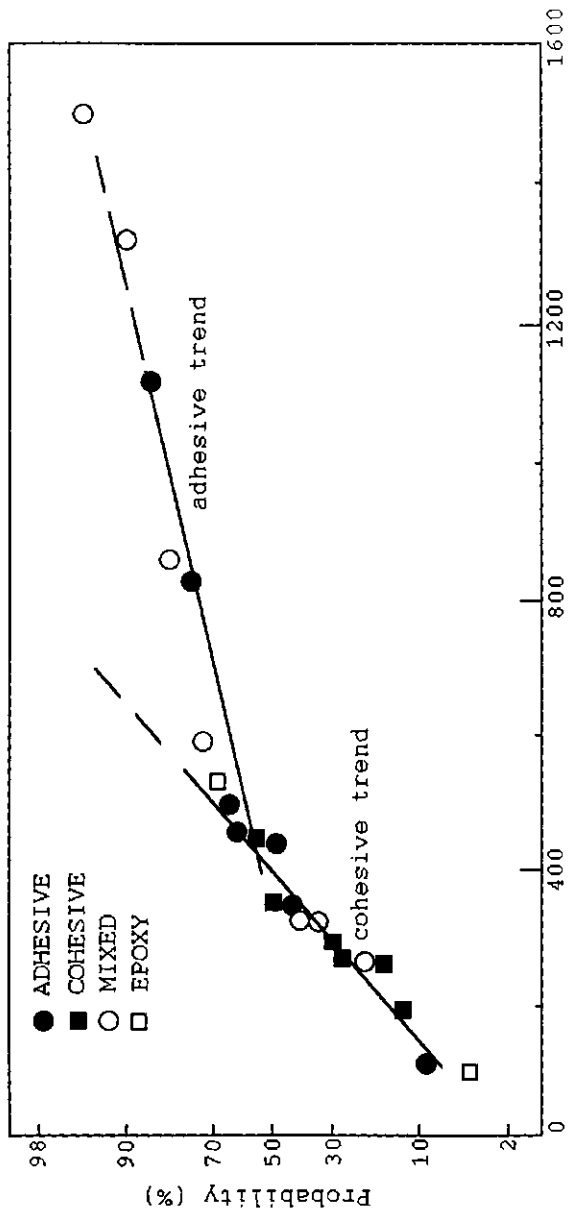

Figure 7-3. Probability plot of stress/strain gradients for a modified ASTM C633-79 test on ZrO_2–8 wt % Y_2O_3/NiCrAlY TBC [29].

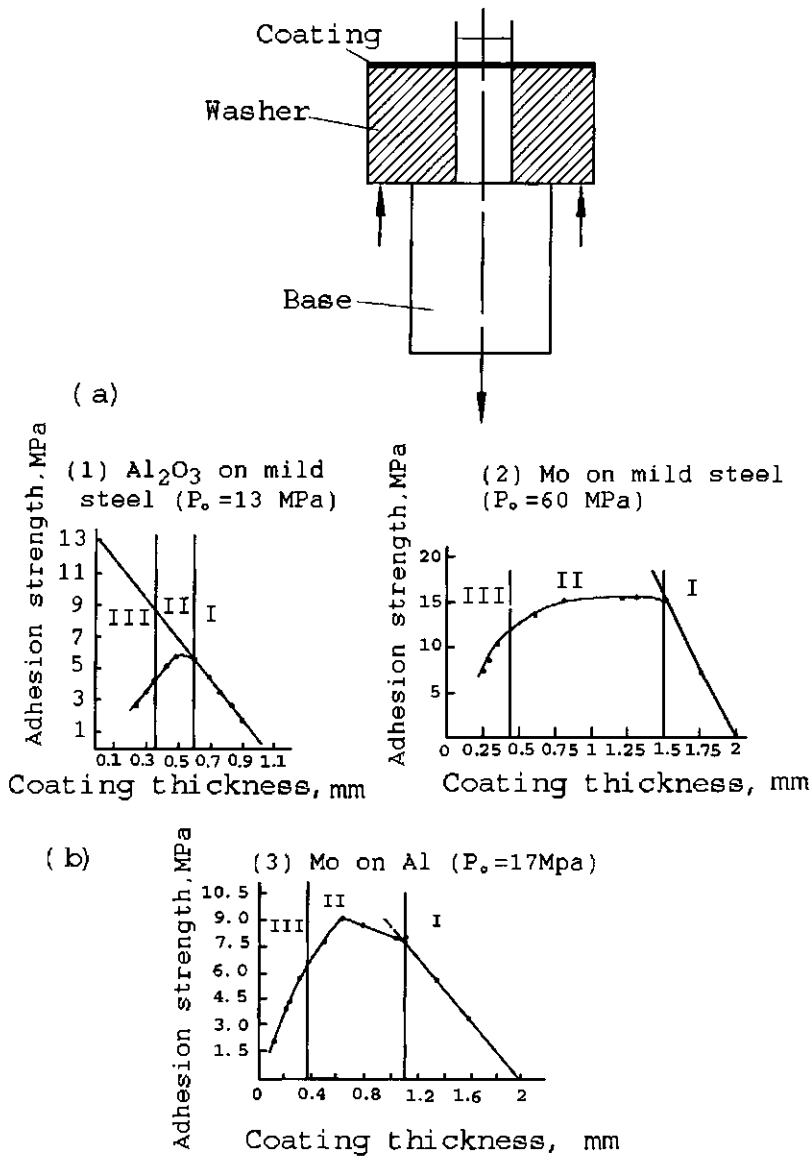

Figure 7-4. Test jig for the Ollard–Sharivker test (a), and adhesion strength versus coating thickness curves (b) for several coating/substrate combinations extrapolated to zero thickness [31].

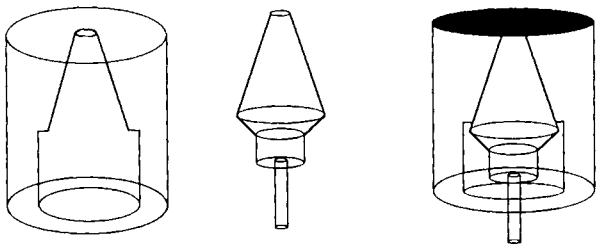

Figure 7-5. 'Pin-hole' test arrangement [36].

interface (zone I). With further decrease of the thickness a transition to cohesion-type stripping occurs (zone II), and finally coating rupture is observed (zone III). For example, the adhesion strength at 'zero' thickness (P_0) is extrapolated for an alumina coating on a steel substrate (coating conditions: 220 A, 85–95 V, argon/hydrogen plasma, argon flow rate 35 l min^{-1}, hydrogen flow rate 4.5 l min^{-1}, stand-off distance 75–100 mm) to be 13 MPa (Fig. 7-4b, 1). This value is comparable to that of a Mo coating on an Al substrate but much lower than that of a Mo coating on steel (Fig. 7-4b, 2 and 3). The geometry of the jig shown in Fig. 7-4a may not be optimal since there is a risk that separation occurs not by tensile forces but by bending or shearing. To account for this the original Ollard test was modified by Roehl [32], Hothersall and Leadbetter [33], Bullough and Gardam [34] and Williams and Hammond [35] (see also Milewski [28]).

A variant of the Ollard test is the 'pin-hole' test (Fig. 7-5). A pin with a diameter of 2 mm is fitted into a massive disc so that the end faces form a planar surface onto which a coating can be deposited [36]. The pin is then pulled off the disc, and the bond strength can be determined by the force at which it detaches from the coating.

Shear tests

These tests are based on the generation of stresses that act tangentially to the coating/substrate interface. It is quite difficult to localize the stresses exactly in the contact plane when the coated workpiece had undergone a preliminary milling or threading treament. But even after customary surface preparation by grit blasting the shear forces occur predominantly in the coating itself and not at the contact plane coating/substrate [37]. Variants of the experimental realization of testing devices have been shown by Milewski [28]. Figure 7-6 shows a device suggested earlier by Metco Inc. [38]. The test is performed on a half-inch wide coating band deposited at the grit-blasted surface of a solid round cylinder. The former is subjected to an axial pressure to shear off the coating from the cylinder. After assembling the two sleeves and the round cylinder, grit-blasting, cleaning and depositing the coating, the set screws will be loosened and the cylinder will be pushed in the direction of the arrow to shear off the coating. The accurately measured load is used to calculate the shear force, and thus the shear strength of the coating. Friable or porous coatings should be given a top coat of stainless steel or Ni–Cr alloy to improve the distribution of the shear stress over the test section. A drawback of this technique is that shrinkage stresses induced into the coating during cooling after spraying will affect the mea-

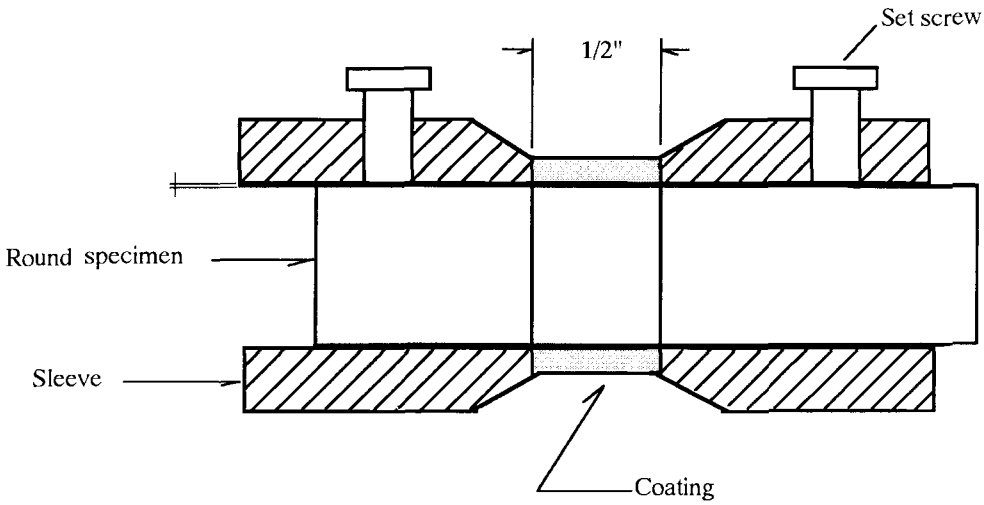

Figure 7-6. Device for measuring the shear strength of coatings (according to Metco Inc. [38]).

sured shear strength to a considerable extent. A shear test deviced by Grützner and Weiss [39] attempts to circumvent this problem.

Peel test

Recently a modified ASTM D-3167 peel test was introduced by Sexsmith and Troczynski [40]. A coating is deposited onto a metal foil soldered to a massive copper block that provides mechanical support and acts as a heat sink. The block, foil and coating assembly is glued to a stiff aluminum plate and the copper block is then removed. Peeling off the foil from the coating (Fig. 7-7) causes a crack to propagate precisely along the coating/foil interface in a controlleable manner because the sample geometry forces the crack tip to move along the interface [41] where it encounters the local least energy path. Although more work is required to fully characterize and evaluate the potential of this adhesion test, its highly controlled crack tip behavior opens up a new way of coating quality testing.

Scratch test

This method uses a Rockwell diamond pressed with increasing load into the coating surface and subsequent pulling away the sample. The ultrasonic signals from breaking of the coating and the interface, respectively as well as the increasing tangential force are measured during loading. Changes in the slope of this force indicate changes of the coating properties, changing in the ultrasonic signal point to coating failure through chipping and spalling as well as loss of adhesion. After the test the trace of the scratch can be evaluated micorscopically. Figure 7-8 shows the recorded tangential force of a VPS (Ti, Mo)C–NiCo coating [42] tested in the range 100–200 N with a CSEM Revetest Automatic Scratch Tester. The coating thickness was 70 μm. The slope of the tangential force versus distance (time) shows a noticeable

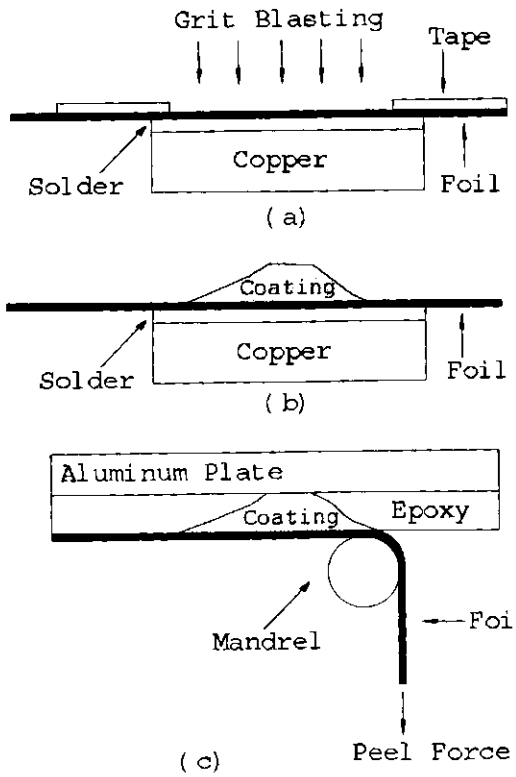

Figure 7-7. Peel test after [40] (a) schematic cross-section of the sample block before spraying, (b) sample block ready to be soldered to Al plate, (c) sample sandwich ready for peel test.

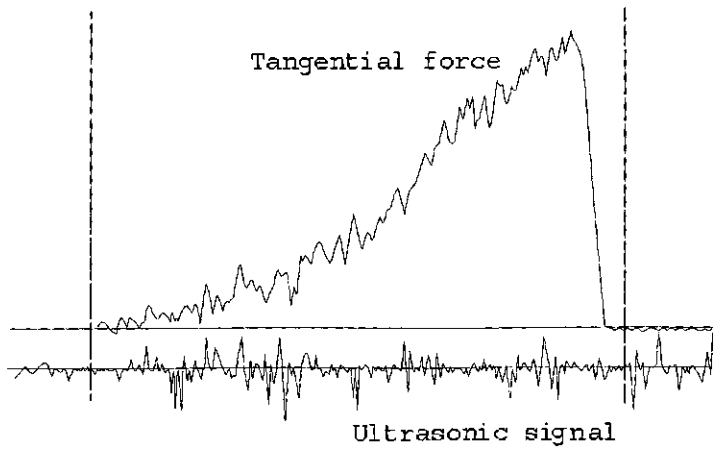

Figure 7-8. Recorded tangential force of a VPS (Ti, Mo)C–NiCo coating and ultrasonic signal obtained with a CSEM Revetest Automatic Scratch Tester [42].

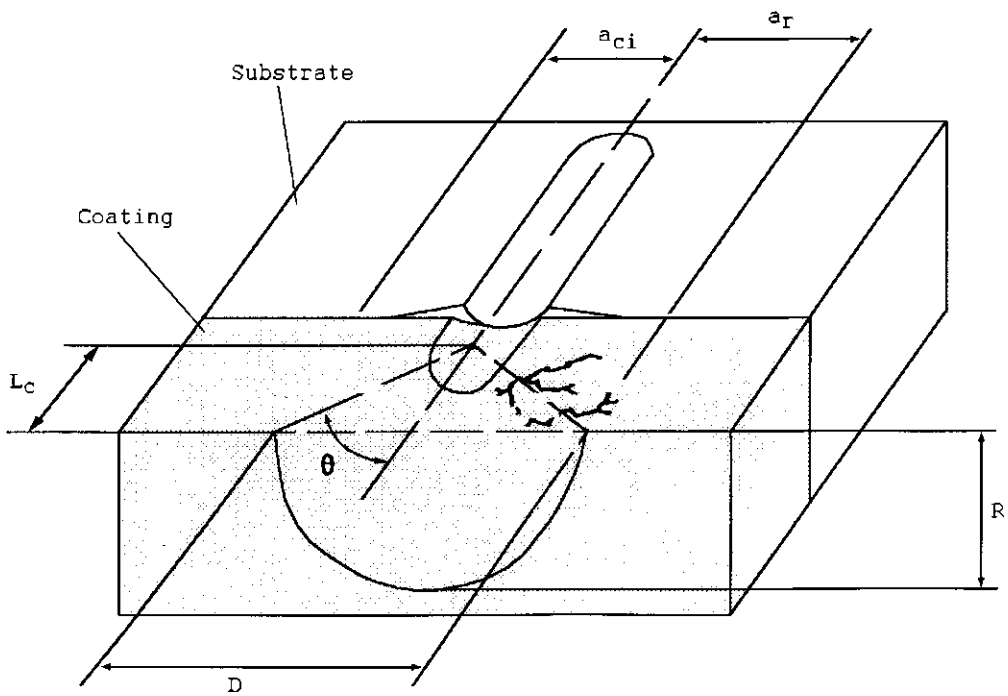

Figure 7-9. Interfacial fracture processes occuring during a scratch test [43].

change. Since the very hard and extremely well-adhering coating did not fail, this change in slope may be attributed to heterogeneities in the coating or even the influence of the substrate because of the rather thin coating. The noisy curve is due to the high surface roughness of $R_a = 30\,\mu m$. The lower wiggly line in Fig. 7-8 is a recording of the ultrasonic signal that also shows no indication of a coating failure but remains within the range of the instrumental noise.

A similar test involves traversing a Rockwell C diamond under a fixed load across a polished cross-section of a coated substrate. Figure 7-9 shows schematically the interfacial fracture processes occuring [43]. At a critical distance (cone depth), L_c, the cracks formed in the coating propagate to the free surface and form a half cone-shaped chip whose depth R is a function of the applied indentor load and seems to be a measure of the coating cohesion. According to Belzung *et al.* [44] the cone depth L_c is related to the indentation load by $F_N = AL_c^{3/2}$ where A is proportional to the fracture toughness, K_c. However, the relationship for APS tungsten coatings was found to be linear by Gudge *et al.* [43].

Ultrasonic tests

With high-frequency ultrasonic waves defects at the coating–substrate interface can be detected and qualitatively related to the coating adhesion. In the second technique, low-frequency ultrasound induces stresses at the interface sufficiently high to

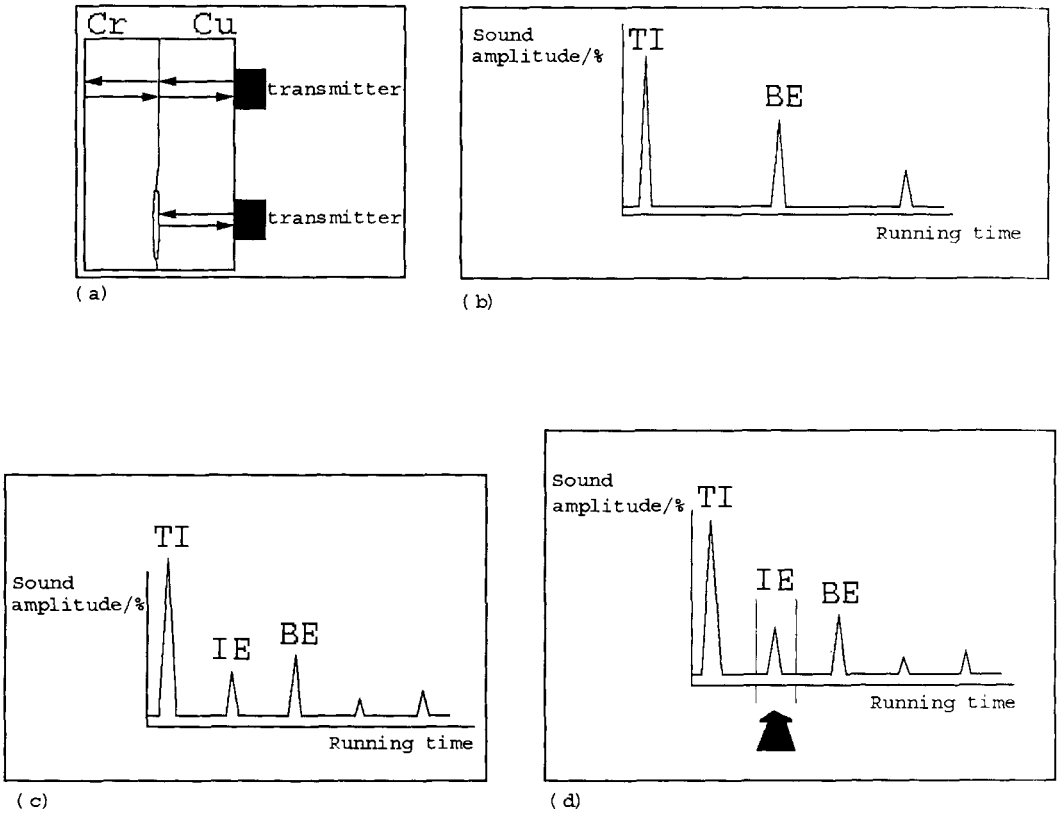

Figure 7-10. High frequency-ultrasonic adhesion test. (a) Geometry of the measuring device, (b) a-scan diagram of a well-adhering chromium coating on a copper substrate, (c) a-scan diagram indicating a coating failure by the presence of an interface echo, and (d) setup for obtaining a c-scan diagram by filtering out the interface echo [46].

detach the coating. The third technique is a combination of the first two, low-frequency ultrasonic energy being used to produce interfacial stresses, and a simultaneously applied high-frequency signal to detect any defects generated by the stressing [23]. Holographic imaging of ultrasonic waves allows imaging of the defects and determination of their size, geometric form, and position. The best sensitivity is obtained if the penetration depth of the induced surface waves is about eight times larger than the coating thickness [45]. Figure 7-10a shows the geometry of the measuring device. As long as there is good bonding between substrate (copper) and coating (chromium) the transmitted signal passes through the interface almost undisturbed. It is first reflected at the back wall and then dected at the copper surface (top). Coating failure is depicted in the bottom part of Fig. 7-10a: the sound waves will be totally reflected at the Cu/Cr interface. Figure 7-10b shows the so-called a-scan diagram of the first case with the transmitted impulse (TI) and the first back wall echo (BE) with its much weaker repetition after twice the original running time. In Fig. 7-10c the situation is shown when a small failure in

adhesion occurs. The waves will be partially reflected at the interface (IE) and only later at the back wall (BE), again with their weaker repetitions. Since only the amplitude of the interface echo is indicative of a good adhesion it is being filtered out of the total spectrum by a narrow strip-shaped window (Fig. 7-10d) and processed separately. Within the bounds of the set window the transmitter is being scanned across the sample and the so-called c-scan diagram is obtained. A useful scanning row distance and step width of 0.5 mm each results in a pixel area of 0.25 mm^2. The best signal resolution in the case of thick VPS-sprayed chromium coatings on copper was achieved using a sound wave frequency of 5 MHz [46]. A specific color can be assigned to each detected amplitude value. Figure 7-11 shows such a color-coded c-scan map of a thick VPS-sprayed chromium coating on an 8 mm thick copper plate. Dark red colors were assigned to 0% coating failure, i.e. maximum adhesion strength, dark purple colors to 100% coating failure, i.e. no adhesion. It can be deduced from the color map that a broad band with decreased adhesion exists passing through the center of the electrospark-machined sample [46, 48].

To quantify the results a combination of the signal amplitude of the interfacial echo (IE) in a c-scan, expressed through the color code, and the adhesion strength obtained destructively by an ASTM C633-79 tensile test can be used. In several cases a good correlation was found [47, 48]. Figure 7-12 shows representative results of the correlation between the mean amplitude of the interfacial echo in percentage calibrated against a coating with no bonding (100%) and the adhesion strength measured by an ASTM C633-79 tensile test [48]. Figure 7-12a is the correlation for an 8 mm thick substrate, Fig. 7-12b for a 5 mm substrate.

To extend the application of ultrasonic testing to samples with complex geometric shapes, recently a robot with five axes was constructed that can change the angle between sample surface and ultrasonic beam automatically [49]. Echo-impulse techniques with an auxiliary reflector, for example by using water as an immersion medium, allow reliable measurement of the adhesion of very thin coatings since the resolution of the reflected signal is much improved. Also, the coupling of the signal head is more uniform [25, 50].

Thermal wave ND scanning

Nonbonded areas perturb the heat flow through the coating into the substrate and thus affect the transient surface temperature [51a]. Bonding defects as small as 300 μm in size can be reliably localized, and such of 150 μm can be detected. Although the test results are affected by scores of parameters the operation does not require a high degree of knowledge of the emissivity of the materials. Thus thermal wave scanning has proved to be a valuable quality assurance tool for thermally sprayed coatings.

Heat is applied to the coating surface by an air-operated heating nozzle. The stream of hot air (500 to 600 °C) is switched between the nozzle and a bypass tube. A computerized infrared radiometer is used to record and store the surface temperature that is affected by the density of bonding defects. Figure 7-13 illustrates a scan of a plasma-sprayed NiCrAlMo bond coat–Al_2O_3/TiO_2 top coat duplex system on a valve stem that failed in service.

With time-resolved infrared radiometry (TRIR) thickness variations and disbonding of zirconia thermal barrier coatings have been studied [51b]. In this case the

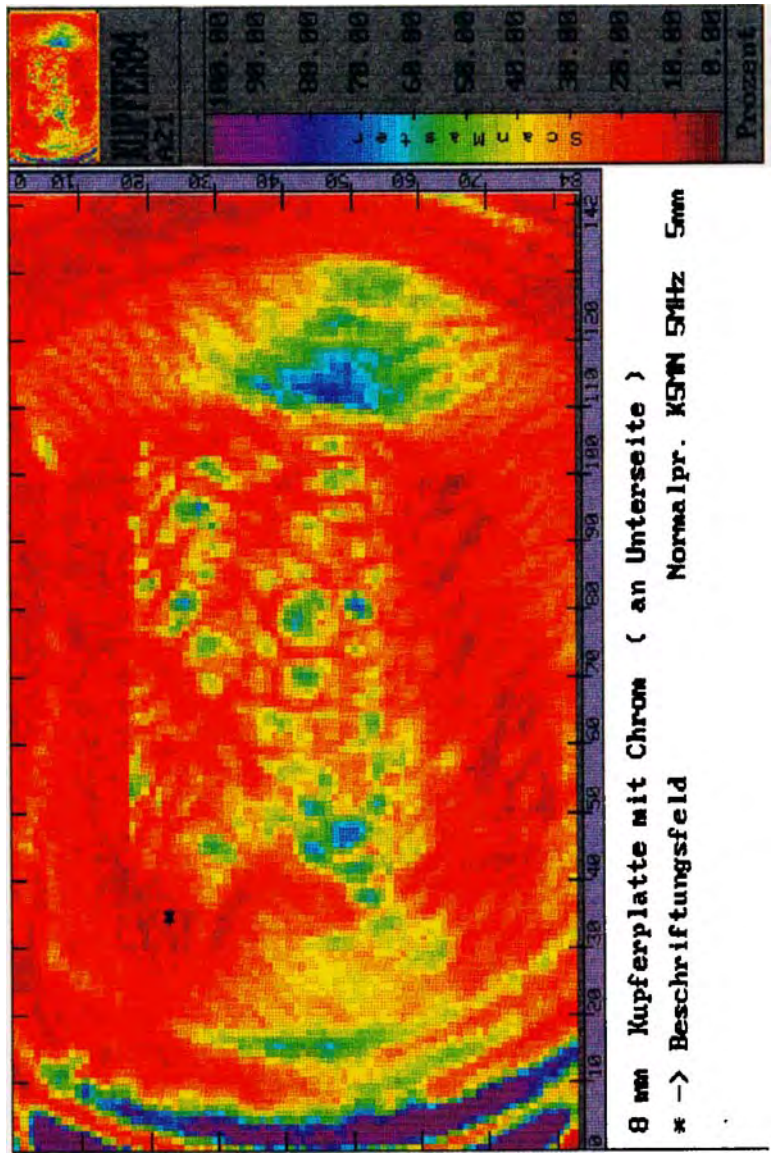

Figure 7-11. Color-coded c-scan map of a thick VPS-sprayed chromium coating on a copper plate [46, 48].

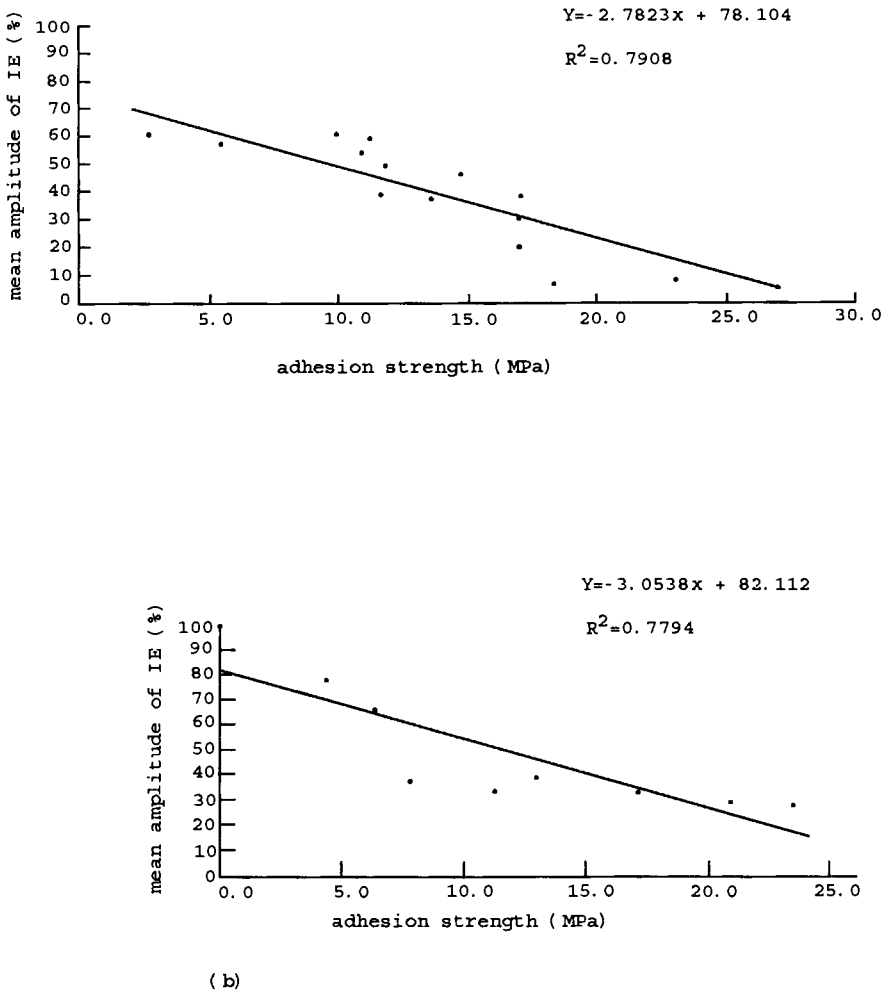

Figure 7-12. Representative results of the linear correlation between the mean amplitude of the interface echo (see Fig. 7-10d) and the adhesion strength measured by ASTM C633-79 for chromium coatings on an 8 mm thick (a) and a 5 mm thick (b) copper substrate [46, 48].

sample is pulse-heated as opposed to the continuous wave photothermal radiometry (CW-PTR) where a continuous modulated heating from a laser source is used. Mathematical modeling of thermal wave NDT of TBCs using numerical finite differences has been attempted by Georgiou *et al.* [52].

7.2.1.2 Macro- and Microhardness Tests

Coating hardness values are often reported to compare the performance of coatings in service as well as the effects of spray variables. These hardness values should gen-

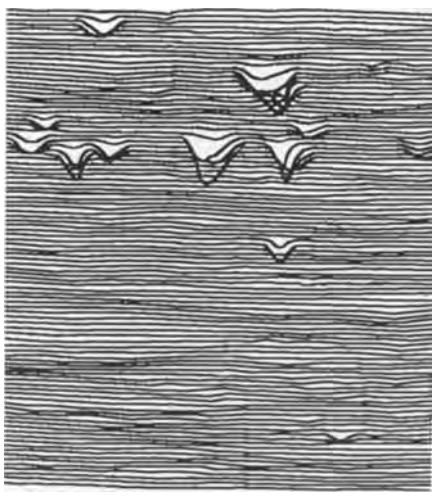

Figure 7-13. Thermal wave ND scan of a NiCrAlMo/ Al_2O_3–TiO_2 duplex coating showing bonding defects [51a].

erally not be considered as a measure of the actual coating strength. For thin and porous coatings with a low cohesion strength macrohardness tests are not applicable. Microhardness tests require careful determination and interpretation so that frequently Rockwell superficial hardness tests are being applied that are simpler to conduct than the standard Vickers or Knoop indentation tests (see below).

Rockwell hardness tests

Procedures for Rockwell superficial hardness tests are laid down in ASTM standard E18-74 [53]. In contrast to a normal Rockwell test this procedure employs smaller loads. The superficial hardness apparatus measures the difference in depth of indentation caused by a minor load (3 kgf) applied first and a major load (15–50 kgf). One unit on the superficial hardness scale represents a penetrator movement of 1 μm between minor and major loads. Most commonly used are the diamond penetrator (N scale) and the ball (T scale). There is no reliable general method of converting hardness numbers from one Rockwell scale to another, or to tensile strengths. The choice of an appropriate scale to use for measuring superficial hardness depends on the hardness and thickness of the coating.

The requirements of the plasma-sprayed coatings to be tested are surface cleanliness and absence of gross imperfections. The impressions of the penetrator should be spaced at least three impression-diameters from each other and from a free edge. Five determinations are normally sufficient to obtain reliable results. A surface finish of 1 μm is recommended for using the 15 N (15 kgf, diamond penetrator) scale. While flat specimens are preferred testing of curved specimens requires correction factors.

Microhardness testing

The standard methods of determining microhardness by indentation of a diamond pyramid are described in ASTM standard E384-73 [54]. Depending on the shape

of the indenter, Knoop and Vickers-type diamonds can be distinguished. In both systems, the hardness number in $N\,mm^{-2}$ is the force exerted on the specimen by the diamond indenter used to produce the impression. In principle, both systems are less affected by porosity than scratch tests based on measuring the indenter travel caused by a specific increase in load. Microhardness tests are usually made transverse to the coating surface, even though loads occuring in service are usually normal to the surface and hardness may vary because of the anisotropy of the microstructure. It is often convenient to make microhardness indentations on specimens prepared for metallographic studies of coatings.

Even though it appears to be relatively easy to perform the measurements the microhardness can be affected by very many parameters including residual stresses, grain size, grain orientation, and the presence of pores and microvoids [55]. Therefore, microhardness is not an intrinsic quantity independent of operating conditions but characterized by the fact that the measured value depends on the applied load. The usual formula used for determining the Vickers hardness is

$$H_V = 1.8544(P/d^2), \tag{7-1}$$

where P is the load in kgf or Newton, and d the diagonal of the indent in mm. In this equation, however, the influence of the load P on H_V is not considered even though it is often observed experimentally that the measured hardness increases as the pyramid load decreases. This nonlinear behavior has been found for SiC [56], TiO_2 [57], Cr_7C_3 [58] and VC [59]. In order to account for the load dependence of the hardness two approaches are usually taken:

(i) *Meyer's approach* [60]: $P = a_m d^n$, (7-2)

where n represents the load–hardness dependence. If $n = 2$, then the hardness is independent of the load. Also, a relation was given by Burnett and Page [61] to describe the hardness in the regime of small loads as $H = qd^{m-2}$, where q is a constant and m the ISE index (indentation size effect).

(ii) *Thomas' approach* [62]: $H = H_0 + (b/d)$. (7-3)

These relations, however, cannot be directly applied to thin films or coatings unless their thicknesses are several times (typically ten times [63]) greater than the indentation depth so that the subsurface deformation beneath the indenter is not influenced by the proximity of interfaces or free surfaces [63, 64]. Those interfaces can be considered for a stratified coating using Bückle's proposal [65] that the hardness should be expressed as a weighted sum of the hardnesses of the different layers. In this spirit a coating/substrate tandem could be considered a two-layer material whose composite hardness is then

$$H_C = \alpha H_F + \beta H_S = H_S + \alpha(H_F - H_S), \tag{7-4}$$

with $\alpha + \beta = 1$, and where H_F = coating hardness and H_S = substrate hardness. The correlation factor α varies from 1 (coating hardness is not dependent on the sub-

strate, i.e. the coating thickness t is at least ten times the indentation depth D) to 0 (coating thickness t is negligible compared to the indentation depth D).

The geometric approach by Jönsson and Hogmark [66] separates coating and substrate contributions to the measured composite hardness by applying a simple 'area law of mixtures':

$$H_C = (A_F/A)H_F + (A_S/A)H_S, \tag{7-5}$$

where A_F = area of indentation within the coating and A_S = area of indentation within the substrate ($A = A_F + A_S$). Figure 7-14a shows the geometry used by Jönsson and Hogmark for their model, and the definitions of A_F and A_S. From geometric considerations an equation can be derived that describes the composite hardness as a function of the ratio t/d using a constant C that takes the value $C = 2\sin^2(11°)$ for hard coatings on very soft substrates or $C = \sin^2(22°)$ for coatings whose hardness is comparable to that of the substrate:

$$H_C = H_S + \{2Ct/d - C^2(t/d)^2\}(H_F - H_S). \tag{7-6}$$

In Eq. (7-6) the parameter t is the thickness of coatings and d is the diameter of the indent ($d \approx 7D$).

Comparison with Eq. (7-4) shows that Jönsson and Hogmark's model is identical to Bückle's when $\alpha = A_F/A = 2Ct/d - C^2(t/d)^2$. Figure 7-14b shows experimental data for thick Cr_3C_2–25% NiCr coatings [67] and the predictions obtained from Bückle's and Jönsson–Hogmark's relations when the fitting parameter α is plotted against the ratio t/d. While Bückle's model fits the data quite well even for thick coatings the Jönsson–Hogmark model does not. However, modifying the original Jönsson–Hogmark model [67] by assuming that the C-value is not constant but varies continuously with t/d according to

$$C = (t/d)^n, \tag{7-7}$$

then the parameter α may be written as

$$\alpha = 2(t/d)^{n+1} - (t/d)^{2(n+1)}. \tag{7-8}$$

Fitting the experimentally measured hardness values to the modified Jönsson–Hogmark model satisfactory results are obtained for a value of $n = 3/4$ (Fig. 7-14c). This value, however, is purely arbitrary and there is no physical confirmation of its validity yet.

A different way to account for the load dependence of the measured hardness is to apply a correction factor to the measured diagonal of the indent (d_{cor}) to obtain a constant absolute hardness [68]. Combining Eqs. (7-1) and (7-3) one obtains

$$\begin{aligned} H &= 1.8544(P/d^2) = H_0 + (b/d) \\ H_{cor} &= 1.8544(P/d_{cor}^2) = H_0 \\ d_{cor}^2 &= d^2 + (b/H_0)d. \end{aligned} \tag{7-9}$$

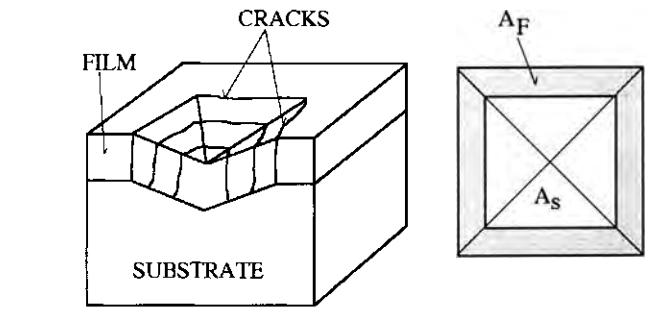

(a)

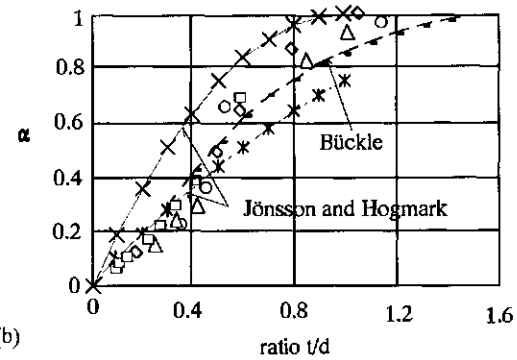

(b)

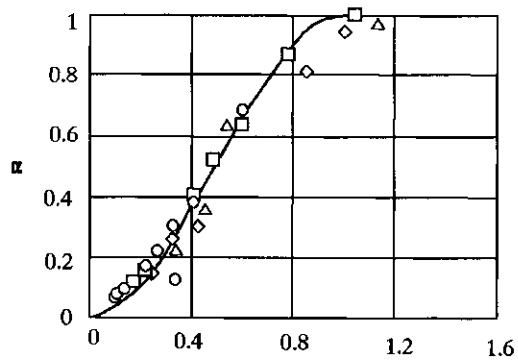

(c)

Figure 7-14. Jönsson–Hogmark 'area law of mixture' model (see text). (a) Geometry and definitions, (b) experimental data for thick Cr_3C_2–25% NiCr coatings fitted to Bückle's [65] and Jönsson–Hogmark's [66] model, (c) experimental data fitted to Jönsson–Hogmark's modified model [67].

Introducing this expression into Jönsson and Hogmark's original equation the following equation is obtained [67]

$$H_C = H_{0,S}[1 - (t/d_{cor})^{n+1}]^2 + H_{0,F}(t/d_{cor})^{n+1}[2 - (t/d_{cor})^{n+1}], \tag{7-10}$$

with the limiting conditions

$$\text{if} \quad t/d_{cor} = 0 \quad \text{than} \quad H_C = H_{0,S}$$
$$\text{if} \quad t/d_{cor} = 1 \quad \text{than} \quad H_C = H_{0,F}.$$

The hardness of a material is related to the plastic work done in creating an indentation. Based on this concept, Burnett and Rickerby [63] developed a model that took into account the relative plastic zone size and the related amount of plastic work. Spherical cavity analysis (Marsh's relation [69]) done on the indentation that creates a hemispherical plastic zone showed that the size of the latter varies with the size of the Vickers indentation according to [70]

$$b/a = c(E/H)^{1/2} \cot^{1/3}\phi, \tag{7-11}$$

where a = indentation semidiagonal, b = radius of plastic zone, c = constant close to unity, and ϕ = indenter semiangle (74°). With this relation a nonlinear 'volume law of mixture' model was suggested by Burnett and Rickerby [63] that incorporated the so-called ISE term (indentation size effect), i.e. the dependence of hardness on load at small indentations as well as the plastic zone size term to yield

$$H_C = (V_F/V)H_F + (V_S/V)\chi^3 H_S \quad \text{for } H_S < H_F \tag{7-12a}$$
$$H_C = (V_S/V)H_S + (V_F/V)\chi^3 H_F \quad \text{for } H_F < H_S, \tag{7-12b}$$

where V_F and V_S are deforming volumes to be calculated using (7-11), and χ is an 'interface parameter':

$$\chi \propto (E_F H'_S / E_S H'_F)^{n/2}, \tag{7-13}$$

where E_F and E_S = modulus of elasticity of coating and substrate, respectively and H'_F and H'_S = characteristic hardness values. The interface parameter is a strong function of the mismatch between the radii of the plastic zone predicted from Eq. (7-11) and also includes deviations from the ideal geometry of the indent. Its value is strongly dependent on the ability of an interface to accommodate the shear stress arising from this mismatch. It may therefore be regarded as a measure of the rigidity of the interface, i.e. the coating/substrate adhesion governing the transmission of shear stresses from a deformed layer to an initially undeformed substrate.

7.2.1.3 Fracture Toughness

It is questionable whether toughness measurements on ceramic coatings actually tell much about the material. Data are often inconsistent, and strength and toughness do

not always respond in the same manner to changes in microstructure of the coating or their interfacial properties. These inconsistencies arise from the sensitivity of the measurements to specimen preparation, i.e. precracking, getting a crack to grow properly in a double-torsion test, and specimen alignment. These problems have been well worked out over the years in more forgiving metals. For example, the fracture toughnesses K_{Ic} of bulk materials measured with the double torsion technique are around 50 MPa $m^{1/2}$ for medium-strength steel, 13 MPa $m^{1/2}$ for Co-bonded tungsten carbide, and 7 MPa $m^{1/2}$ for Ca-stabilized zirconia (double cantilever beam test).

A four-point bending test can provide at least some information on the toughness of plasma-sprayed coatings [71]. The test consists of placing a coated beam in pure four-point bending with the coating in tension and recording cracks by acoustic emission (AE) with a piezoelectric transducer attached to the surface of the coating. Simultaneously the coating strain is monitored by strain gages, and the test results are presented as strain to fracture (STF). It was found that for WC/Co coatings the STF (toughness) depends strongly on the residual stresses present (see Sec. 5.5.5) but neither appreciably on the microhardness nor the metal content of the coating. The acoustic signals picked up by the transducer occur at four different amplitudes thus suggesting different cracking mechanisms. Early in the test, low amplitude events around 50 dB took place that were related to pre-cracking or microcracking. On release of the bend stress no visible damage in the test specimen could be discerned. The second type of noise at greater 100 dB amplitude are true coating cracks as confirmed by a close to one-to-one correlation between high amplitude events and the number of macrocracks in the coating following testing. During macrocracking the number of low amplitude events increase strongly. They are considered reflections of the stress wave developed at the crack front and thus are not related to changes in the material. The last type of AE events around 80 dB may be related to cracks that propagate through fewer lamella than the cracks causing the 100 dB events.

Bend tests can also be used to determine the probability of rupture of ceramic coatings using Weibull analysis [72]. Free standing samples of PSZ with a length L and thickness d were subjected to a three-point bend test, and the modulus of elasticity, E and the mechanical strength, σ were determined from the moment of inertia, I:

$$E = FL^3/48fI, \tag{7-14}$$

where F = force, f = displacement of the center point, and

$$\sigma = FLd/8I. \tag{7-15}$$

The probability of rupture Pr of the zirconia ceramic is given by

$$Pr = \exp[-(\sigma/\sigma_0)^m], \tag{7-16}$$

where σ is the applied stress, σ_0 the normalized stress below which 63% of the sam-

ples fail, and m the Weibull modulus. Eq. (7-16) can be written in the following form

$$\ln[\ln(1/1 - Pr^i)] = m \ln(\sigma_r^i) + \ln(1/\sigma_0^m), \tag{7-17}$$

where i refers to the experiment number i when all experiments are classified starting from the lowest values σ_r to the highest, and where Pr^i is estimated by

$$Pr^i = (i - 0.5)/n \tag{7-18}$$

with $n =$ total number of experiments. By plotting the left-hand term of Eq. 7-17 against $\ln(\sigma)$, the slope of the resulting straight line determines the Weibull modulus m, and the intersection with the $\ln(\sigma)$-axis results in σ_r.

Using the scratch test described above and data obtained for the coating fracture toughness from the half-cone fracture shown in Fig. 7-9, Lopez *et al.* [73] estimated the coating cohesion for plasma-sprayed alumina, alumina–titania, chromium oxide, chromium carbide–NiCr, and WC–Co coatings.

7.2.2 Tribological Properties

There are three primary types of wear: adhesive, abrasive, and erosive. Other composite types of wear include surface fatigue, fretting and cavitation erosion. Since there is no universal type of wear, there is also no universal method or machine for testing wear. Laboratory tests are aimed at simulating service conditions and consider the position of the fixed or loose abrasive, the size, shape and hardness of the dominant abrasive, the direction and speed of relative motion during abrasion, and the contact pressures or loads in the system.

A rubber-wheel test (ASTM G 65) simulates low-stress or scratching abrasion with loose abrasive. Gouging abrasion is tested in a jaw-crusher (ASTM G 81). Sliding wear tests (ASTM G 77, ASTM G 83) and erosive wear tests (ASTM G 73, ASTM G 76) are generally applied to metals and plastics. Tests to evaluate the wear in ceramics are based on the pin-on-disc (POD) concept. In the microwear pin-on-disc apparatus, a diamond pin with a predetermined applied load rides on the rotating specimen (coating). In the macrowear tester, two freely rotating wheels (Taber apparatus) ride of the rotating specimen assembly that consists of twelve trapezoidal-shape sections held together by a circular ring on the outside edge and a disc in the center. A general discussion of tribological properties of thin films and coatings, thick coatings, and hardfacing has been presented by Kelley *et al.* [74].

Since the wear behavior of coatings is strongly influenced by composition, microstructure, residual stresses and surface conditions, tribological properties of coatings must be evaluated under conditions that match as closely as possible the actual in-service conditions [75]. As this is generally not possible, wear model tests are applied that simulate the very complex wear processes in technical tribosystems under simplifying conditions at ambient conditions [76]. As a consequence, application of the results of such wear model tests to the real world is generally unsuccessful.

To illustrate the degree of complexity, Fig. 7-15 shows the methodology of wear tests for tribomaterials [76]. Wear mechanism maps are particularly useful to reveal the relationships between interaction parameters and dominant wear mechanism [75].

7.2.2.1 Simulation of Basic Wear Mechanisms

These quality assurance procedures involve testing for adhesive and abrasive wear as well as for long-term fatigue and erosive wear. The tests permit to investigate the local behavior of the coating/substrate tandem system subjected only to those basic wear mechanisms. Evaluation of existing models for abrasive wear and impact erosion was performed by Dimond *et al.* [77] to reconcile the results of laboratory wear tests and theoretical models to the true wear performance of a material in service.

Adhesive wear

Friction is generated by local adhesion and subsequent separation of the contact faces of a tribological couple. The contact of the two surfaces does not occur along the entire geometrical surface area A_0 but only with the fraction

$$A/A_0 = (\sigma/H)R, \tag{7-19}$$

where A is the effective contact area. This ratio increases with increasing compressive stress $\sigma = F/A_0$ and surface roughness R, and decreasing hardness H of the materials. The friction coefficient μ is given by $\mu = F_R/F$, where F_R = frictional force = $(d\gamma/dx)A$ and F = compressive load. The energy dissipation γ per glide distance x, i.e. $d\gamma/dx$ in the effective contact area A is the actual physical reason for dry friction [78].

The test of adhesive wear uses the adhesion tendencies of tribocouples to determine an 'adhesion number' $\mu_{v,ad}$ that is numerically different from the friction coefficient defined above [76]. The adhesion number is determined as the ratio of the tangential force F_T to the normal force F_N of a tribosystem consisting of a counterbody attached to a torque rod transferring the torsional momentum to the coating surface that is pressed against the conterbody with the normal force F_N. The torsional momentum is only maintained by adhesive forces, and when the normal force F_N is being relaxed the counterbody slides back to its starting position. From the displacement diagram both F_T and F_N and therefore $\mu_{v,ad}$ as a measure of the adhesive tendency of the tribocouple can be determined.

Abrasive wear

Using the scratch tester mentioned above information on the abrasive wear properties of coatings subjected to the indentation load of a Vickers diamond pyramid can be obtained. The indenter is pressed against the surface of the coating with the normal force F_N and at the same time the sample is being moved relative to the indenter for a distance L_R with a velocity v_R. The measured tangential force F_T is related to

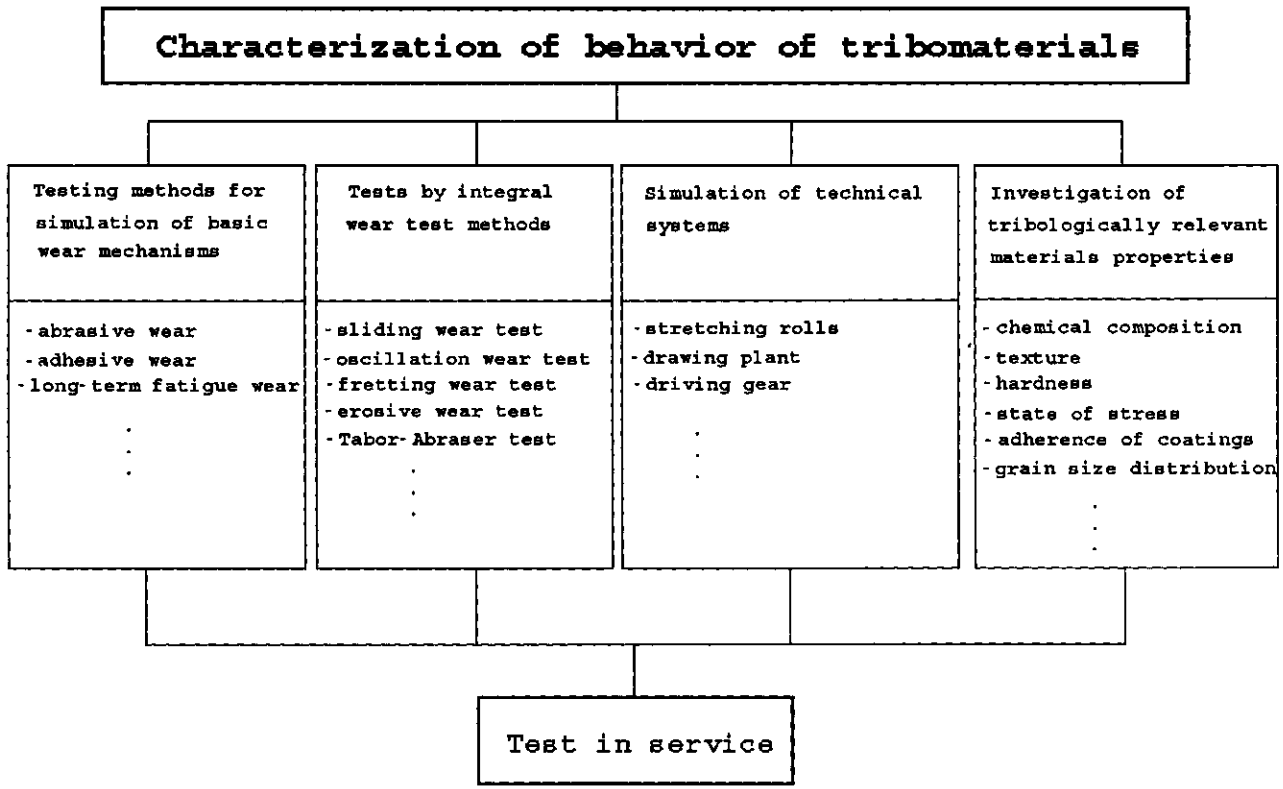

Figure 7-15. Methodology of wear tests for tribomaterials [76].

the volume of the produced scratch that can be determined by laser beam tracing and the scratch energy density W_R is obtained in J mm^{-3}:

$$W_R = (F_T L_R)/(A_R L_R), \tag{7-20}$$

where A_R is the so-called scratch square, i.e. the cross-section of the scratch. Note that the expression in the denominator of Eq. 7-20 is the volume of the material removed by the scratching operation.

Frequently problems occur due to microploughing, microcutting and -chipping and particle pull-out that tend to obscure the scratch traces. Figure 7-16 shows a scratch produced in a (Ti, Mo)C–NiCo coating on a mild steel substrate and its laser-generated profile. The scratch energy density was calculated to be 5.2 J mm^{-3} [42].

The most frequently applied abrasive wear test is the dry sand–rubber wheel abrasion test according to ASTM G65 [79]. This simple test measures material losses occuring when a coated sample surface is being pressed with a defined force against a steel wheel whose circumference is lined with rubber. Into the gap between the sample and the wheel sand (Ottawa sand) or other abrasive materials are being fed from a hopper reservoir with a constant flow rate (Fig. 7-17). After 2 000 revolutions of the wheel the sample is removed and weighed. The loss of material is a measure of the abrasive resistance of the coating.

Long-term fatigue wear

In this test the cylindrical sample to be tested is pressed against a curved counterbody disc whose diameter is ten times that of the cylindrical sample (Fig. 7-18). The curvature of the rotating disc is different in two perpendicular directions in order to minimize the contact surface between disc and cylindrical sample. The load m_A applied generates the normal force F_N. The critical number of load reversals as well as scratch and pit formation are evaluated. This test is still in the development phase [76].

Erosive wear

A widely applied test for erosive wear of ceramics and ceramic coatings is the impact abrasion/solid particle erosion test based on depth of penetration produced by a standard sand or grit blast (ASTM G76-83). Erosion is a mechanism of wear resulting from the impact of abrasive particles on a target material [80, 81]. The erosion rate of a plasma-sprayed coating is a complex function of many variables including the size, shape, velocity, flux and angle of impact of the impinging particles and such coating properties as hardness, grain size diameter (Orowan–Petch relation), porosity (Ryshkevich–Duckworth equation), ductility or fracture toughness. Figure 7-19 is a diagram of the erosion test apparatus according to ASTM G76-83. A screw-feed type metering system releases controlled amounts of an erodent (sand, glass beads, crushed alumina, carborundum etc.) into a flowing gas stream. Particles delivered are picked up in the stream and accelerated through a tungsten carbide nozzle before being directed at the coating surface. Figure 7-20 shows the schematic sequence of

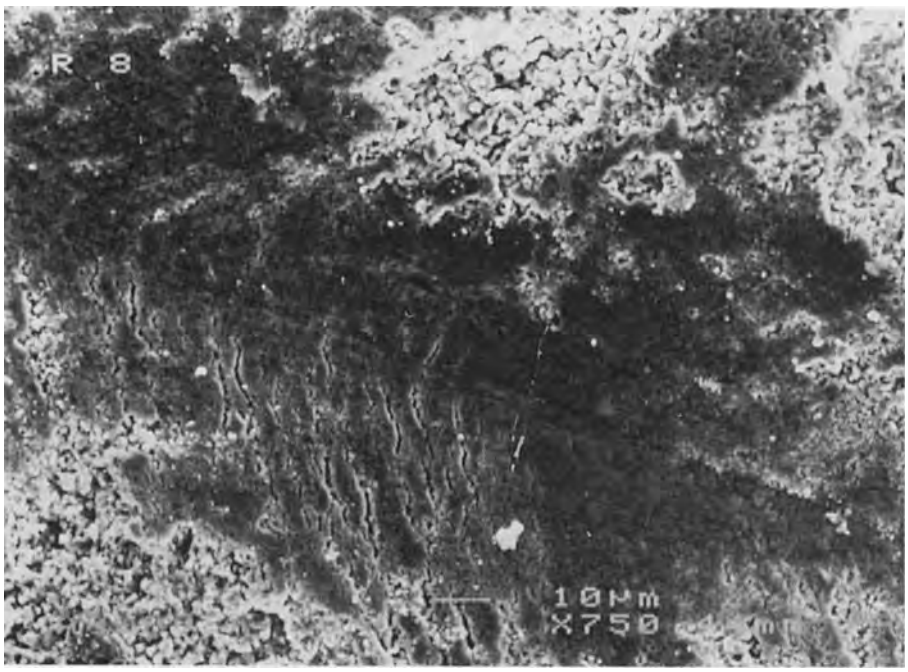

(a)

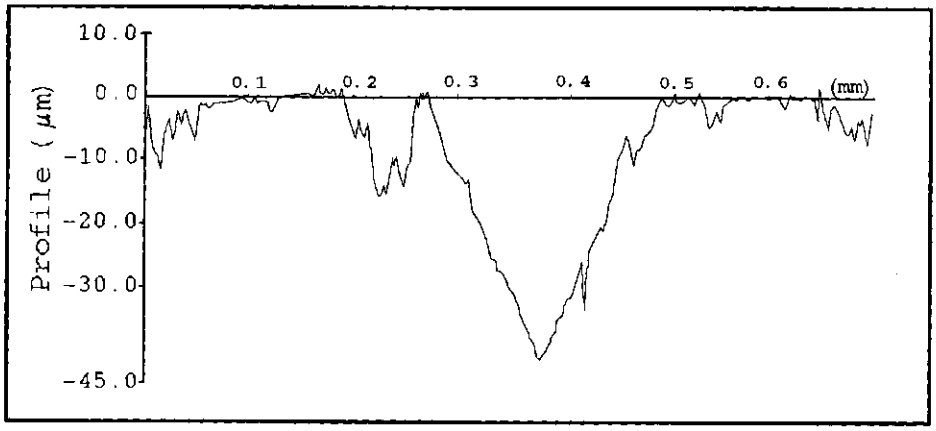

(b)

Figure 7-16. Scratch produced with a diamond indenter in a (Ni, Mo)C–NiCo coating (a) and its laser-generated profile (b) [42].

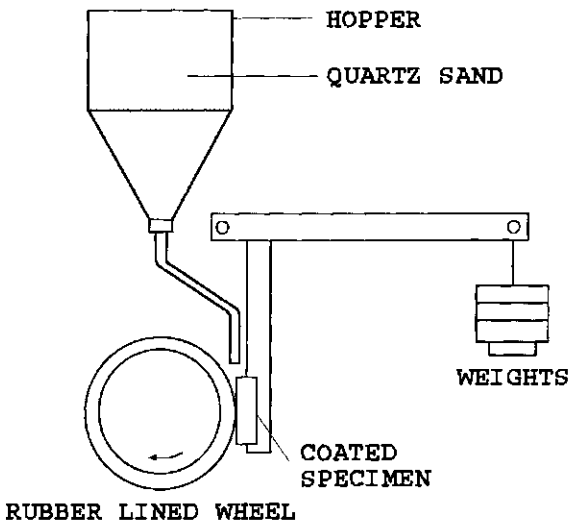

Figure 7-17. Dry sand–rubber wheel abrasion test device according to ASTM Designation G65 [79].

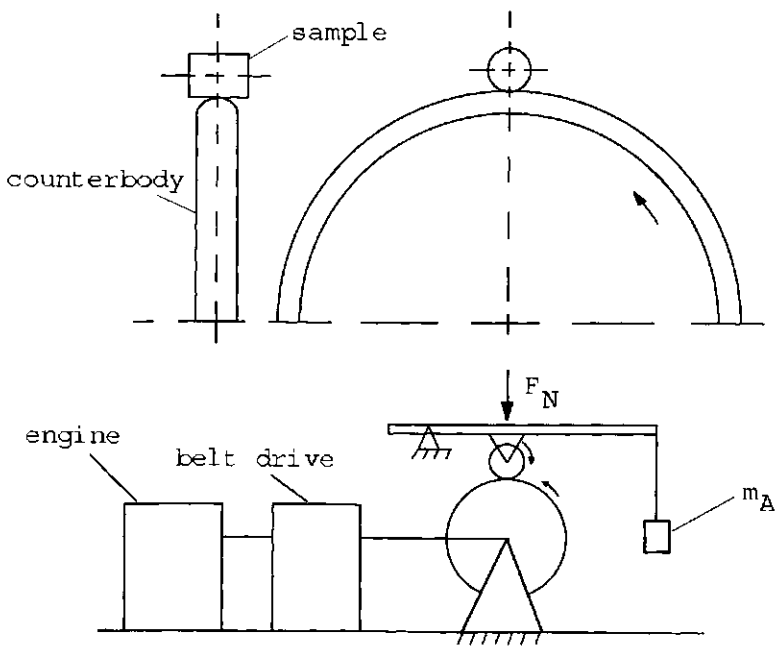

Figure 7-18. Long-term fatigue wear test device [76].

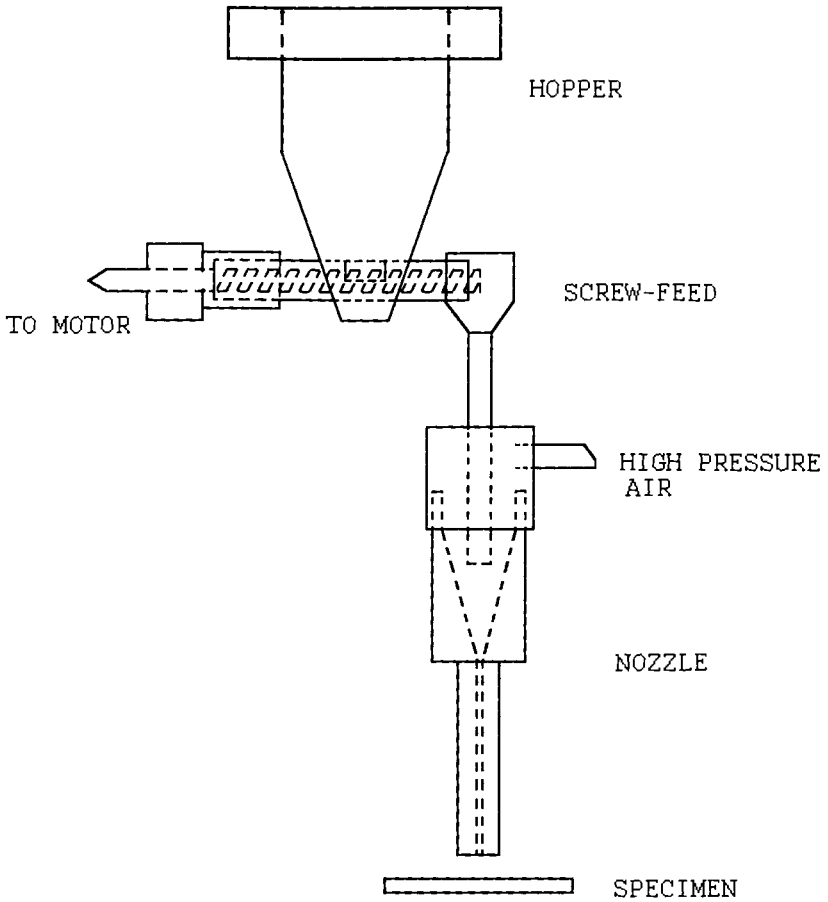

Figure 7-19. Solid particle erosion (SPE) test device according to ASTM Designation G76-83.

events for impact of a high-energy erodent particle [82]. The highly accelerated particles are able to penetrate the coating completely and to deform the metallic substrate underneath in a ductile manner by cutting and ploughing. Release of the deformation energy results in a chipping mechanism that removes parts of the coating and thus exposes the substrate to environmental attack by corrosion or abrasive wear. Maximum loss of coating would be expected at shallow impact angles in the 15–30° range (Fig. 7-21, [83]) and the velocity dependence exponent of erosive wear would be about 2.0 to 2.5 [82].

It should be pointed out that this is an important mechanism of the erosion of high-pressure turbine blades and valve components of fossil-fuel fired power plants [84, 85]. Hard particles of magnetite scale formed at elevated temperature by reaction of steam with ferritic alloy boiler tube material can exfoliate from the interior surfaces of the boiler tubes during boiler transients (startup and cooldown cycles).

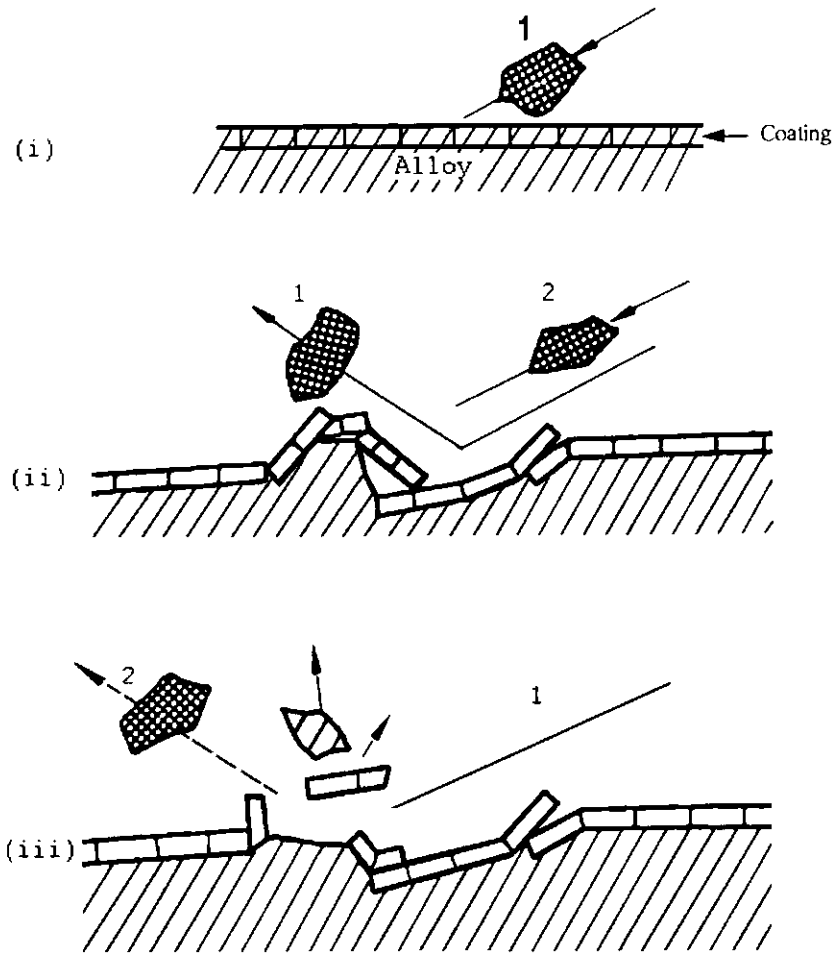

Figure 7-20. Schematic sequence of events occuring during the impact of a high-energy erodent particle onto a plasma-sprayed coating [82].

This solid particle erosion attacks the blade airfoil at various impingement angles when passing through the turbine and also erodes any other component of the steam path. By this mechanism protective coatings along the steam path such as plasma-sprayed $80Cr_3C_2/20$(NiCrMo) coatings [86] can be completely destroyed.

7.2.3 Chemical Properties

Performance specifications of coatings for high-temperature applications, for example gas turbine blades, combustor cans, ladles and tundishes for metal casting etc. require quality testing that must be able to simulate the severe service conditions at

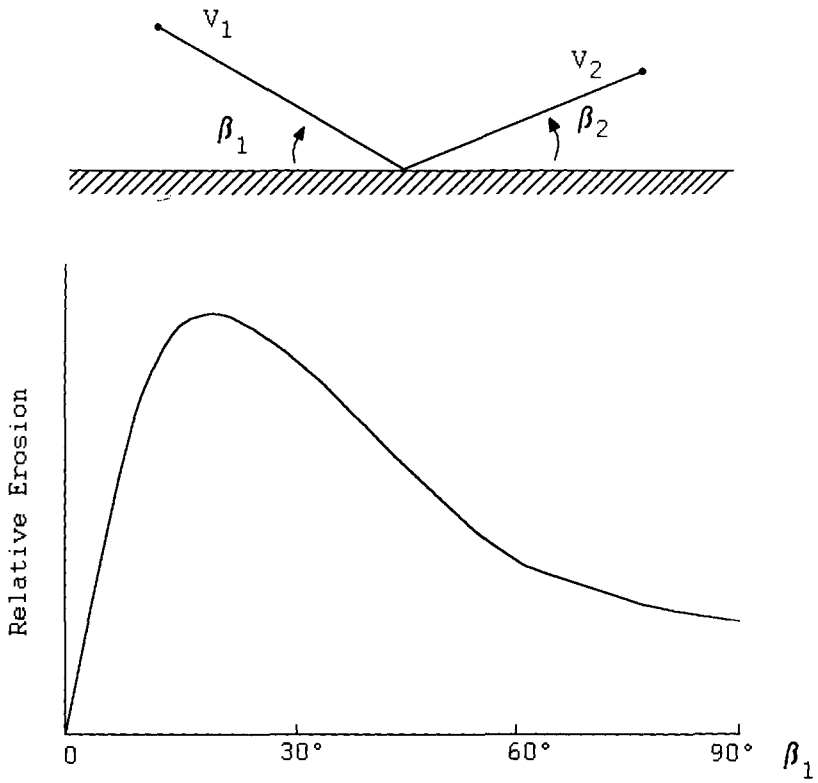

Figure 7-21. Dependence of relative erosion rate on the impact angle [83].

which the coated parts are supposed to function. A comprehensive review of production and performance evaluation of high-temperature coatings has been given by Nicoll [87]. Since the coatings are subjected to synergistic effects of mechanical stresses, temperature and corrosive environment small coating failures can lead to catastrophic destruction of components of engineering systems. Environmental test considerations include the gas temperature, composition, pressure, velocity and temperature cycling. Also, contaminants such as sulfates and vanadates as well as particulate matter can lead to deposition and corrosion, and also destructive erosion effects. Figure 7-22 shows several of such degradation mechanisms that can affect plasma-sprayed stabilized zirconia–NiCrAlY duplex coatings [88, 89]. While in combustion environment hot corrosion of ceramic components such as SiC, Si_3N_4, and SiAlON occurs in a manner similar to dry oxidation, i.e. under formation of a protective SiO_2 surface layer, inpurity gaseous species such as Na_2SO_4 and NaCl can condense at the surface of engine components at temperatures as high as 1100 °C and lead to severe corrosion, pitting, and strength reduction [90, 91].

To select a proper protective coating system for high-temperature applications, three main factors must be considered: the applications, the structural alloys to be

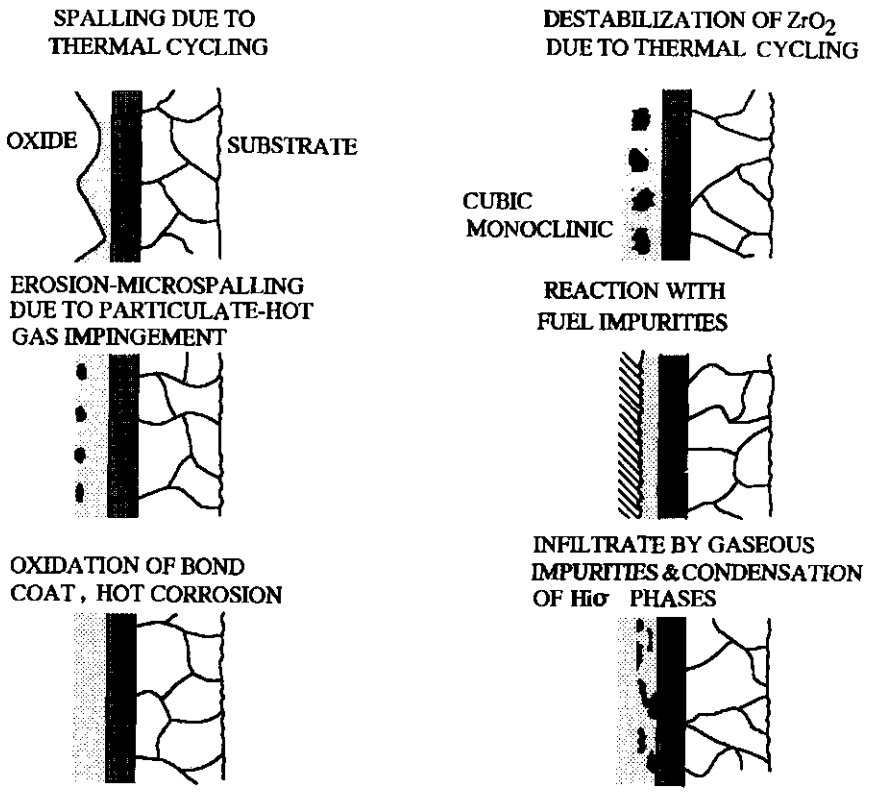

Figure 7-22. Degradation mechanisms of stabilized ZrO_2/NiCrAlY thermal barrier coatings (TBC) [88].

protected, and the coatings themselves. Figure 7-23 show schematically the interactions of mechanical properties, coating processes, and the environmental attack the system is subjected to. The design of the component determines the service stresses, maximum operation temperatures, and service environment. Alloy properties are controlled by chemistry, processing and the resulting microstructure that can also control the high temperature stability [87]. Enviromental considerations include the gas temperature, composition, pressure stream velocity, and temperature cycling. Since materials at high temperatures are subject to corrosion phenomena, e.g. oxidation, hot corrosion/erosion or carburization tests to evaluate high temparature performance of coating systems have to account for these interactions. Degradation of coatings also involve creep [92, 93], and low-cycle [94] and thermal fatigue [95].

All evaluation tests at various stages of the develoment of a high temperature protection coating system can be grouped according to their cost, number of tests required and their extrapolation risk. Thus *screening tests* require many samples at comparatively low cost performed as crucible tests at isothermal exposure. *Bench-scale tests* such as creep testing need fewer samples but the costs are increased. *Com-*

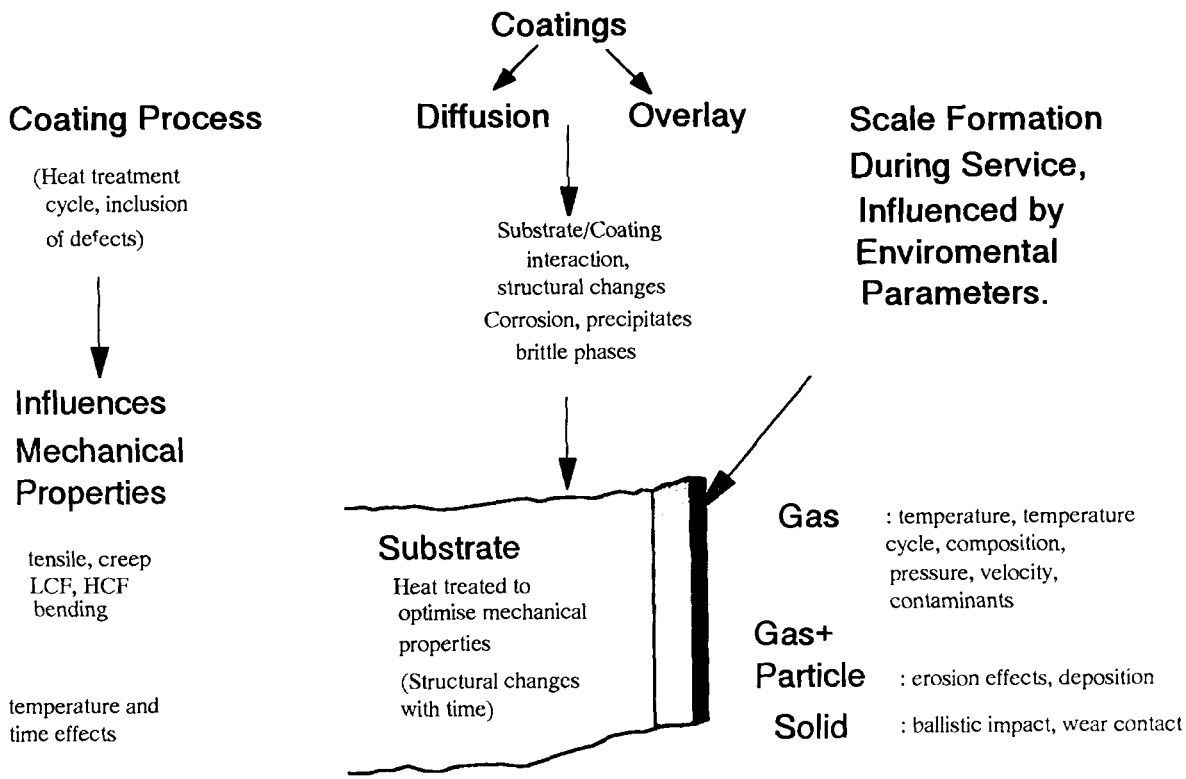

Figure 7-23. Interaction of mechanical properties, coating processes, and environmental attack for high temparature-resistant coatings [87].

ponent tests use a simulated service environment such as burner rig testing for gas turbine blades. Finally, tests designed to provide *service life prediction and systems verification* are most expensive, require but a few samples, and are performed in a pilot plant or for 5000 h in a stationary gas turbine. Figure 7-24 shows a typical coating evaluation program for the evaluation of new coating systems for industrial gas turbines [96] that includes a combination of short-term complex environmental exposure, mechanical tests and long-term laboratory test for structural stability (up to 10 000 h).

7.2.3.1 Chemical Corrosion Evaluation Tests

The short-term chemical corrosion tests in their required complexity are shown in Fig. 7-25 [97]. Since corrosion resistance of a coatings depends to a large extent on the rate of formation of a protective scale, the simplest method is to expose the coating isothermally to either air or oxygen, to atmospheres containing hydrogen sulfide, sulfur dioxide or trioxide, or to 'coal' atmospheres (methane). The weight change of the sample will be measured, and the nature of the scale formed be determined by X-ray diffraction analysis. Cyclic modes of testing are utilized to introduce thermal strain between coating and substrate, and coating and scale. Abrupt weight changes measured with a thermal balance may indicate spalling and chipping of the scale. Addition of impurities to the corrosive environment accounts for the presence of chlorides, sulfates and vanadates in the combustion gases. Such tests are usually performed as immersion tests where the coated sample will be immersed in an appropriate salt melt. The extent of attack can be determined from thickness changes on the metallographic cross-section or from weight loss after descaling [98]. Frequently the attack during such a crucible test would appear to be more severe than that encountered during normal service conditions of the coating. The reasons for this are manifold. For example, the salt composition is often unrealistic, the oxidation potential is low, and the test is static. To overcome these problems other test schedules were devised such as the salt-shower test [99], the synthetic slag test [100], and the modified Dean test [101].

7.2.3.2 Burner Rig Test

This test simulates reasonably well the severe conditions at which a coating has to function in a gas turbine [102]. Such a test rig consists of a combustion chamber taken from a small turbine into which fuel and compressed air is fed in the usual manner. Contaminants are supplied either to the fuel or to the air, or can be sprayed directly into the combustion chamber onto specimen coupons to be tested. These coupons are either stationary or rotate. Variables to be tested include coating temperature, gas pressure, velocity, dwell time, contaminant concentration and composition, and also the fuel-to-air ratio [87]. The samples are investigated after the test by measuring weight loss and/or penetration depth of the corrosive gases. To increase the realistic evaluation of coating systems the burner rig test can be cycled [103].

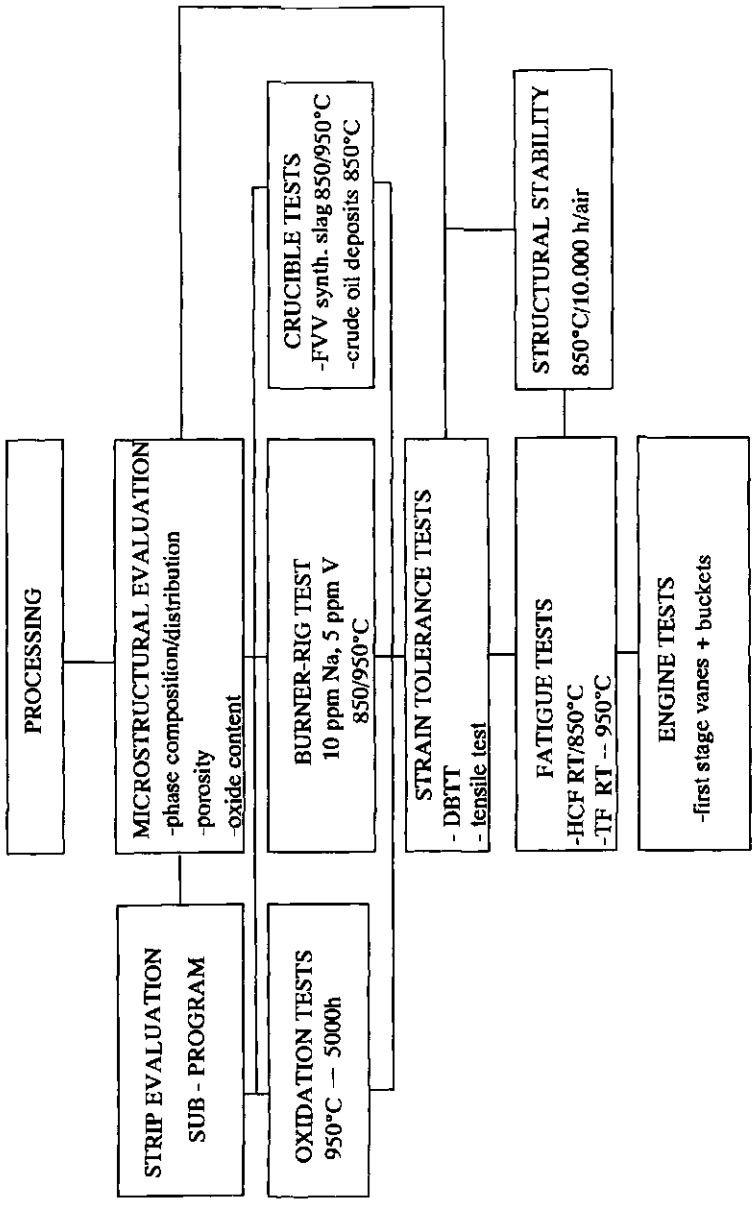

Figure 7-24. Typical coating evaluation program for coatings applied to stationary gas turbines [96].

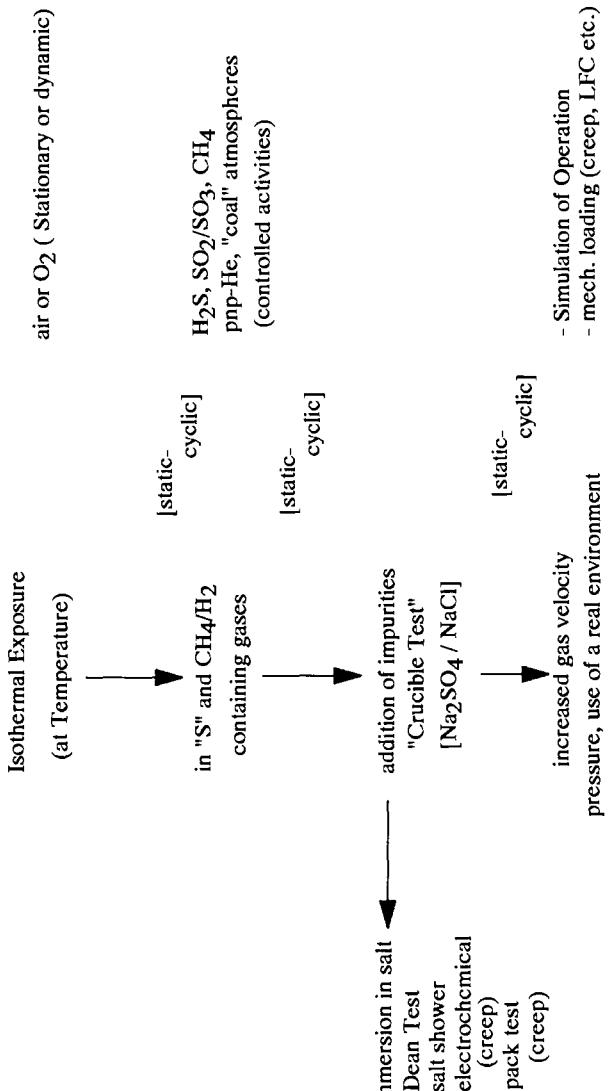

Figure 7-25. Complexity of short-term chemical corrosion tests [97].

References

[1] B. Keys, T. Miller, *Acad. Managem. Rev.* **1984**, *9*, 342.
[2] J. Fakuda, *J. Gen. Managem.* **1986**, *11*, 16.
[3] H. M. Wadsworth, K. E. Stephens, A. B. Godfrey, *Modern Methods for Quality Control and Improvement*, Wiley, NY, USA, **1991**.
[4] D. C. Montgomery, *Introduction to Statistical Quality Control*, Wiley, NY, USA, **1991**.
[5] J. M. Juran, *Planning for Quality*, The Free Press, NY, USA, **1988**.
[6] R. C. Camp, *Benchmarking: The Search for Industry Best Practices that Lead to Superior Performance*, Quality Press and UNIPUB/Quality Resources, **1989**.
[7] E. J. Hay, J. Zonderman, *Just in Time Manufacturing: How the JIT System Can Decrease Costs, Increase Productivity and Enhance Quality*, Wiley, NY, USA, **1988**.
[8] M. Owen, *SPC and Continuous Improvement*, Springer-Verlag, UK, **1989**.
[9] J. R. Hauser, D. Clausing, *The House of Quality*, Harvard Business Review, May–June, **1988**.
[10] G. Pouskouleli, T. A. Wheat, in: *Ceramic Coatings – A Solution Towards Reducing Wear and Corrosion* (ed. R. B. Heimann), *Trans. 17th CUICAC Workshop*, Quebec City, 2 October, **1991**.
[11] W. Ouchi, *Theory Z*, Addison-Wesley, MA, USA, **1981**.
[12] J. M. Juran, *Juran's Quality Control Handbook*, McGraw-Hill, NY, USA, **1988**.
[13] W. E. Deming, *Out of the Crisis*, MIT Press, Cambridge, MA, USA, **1986**.
[14] P. B. Crosby, *Quality is Free*, McGraw-Hill, NY, USA, **1979**.
[15] ISO 9001, *Quality systems-model for quality assurance in design/development, production, installation and servicing*, **1994**.
[16] K. Ebert, C. M. Verpoort, *Proc. 14th ISTC '95*, Kobe, Japan, 22–26 May, **1995**, p. 1191.
[17] *A Plasma Flame Spray Handbook* (ed. T. J. Roseberry, F. W. Boulger). *Final Report No. MT-043* (March 1977) *to Naval Sea Systems Command*, Naval Ordnance Station, Louisville, KY, USA, **1977**.
[18] *Standard Specification for Wire-Cloth Sieves for Testing Purposes*, ASTM Designation E11-70. (Feb. 15. 1973).
[19] *Standard Test Method for Sieve Analysis of Granular Metal Powders*, ASTM Designation B214-66, 1966 (reapproved **1970**).
[20] *Standard Method for Subsieve Analysis of Granular Metal Powders by Air Classification*, ASTM Designation B293-60 (reapproved **1970**).
[21] H.-D. Steffens, K.-N. Müller, *Adhäsion* **1972**, *2*, 34.
[22] (a) D. T. Gawne, B. J. Griffith, G. Dong, *Proc. 14th ITSC '95*, Kobe, Japan, 22–26 May **1995**, p. 779; (b) R. A. Miller, W. J. Brindley, C. J. Rouge, G. Leissler, *NASA Tech. Briefs*, **1993**, *17*, 56.
[23] D. Davies, J. A. Whittaker, *Metall. Rev.* **1967**, *12*, 15.
[24] L. Pawlowski, *The Science and Engineering of Thermal Spray Coatings*, Wiley, Chichester, **1995**.
[25] R. Frielinghaus, G. Schmitz, U. Wielpütz, *Proc. TS '90*, Essen, **1990**, DVS 130, p. 147.
[26] *Standard Test Method for Adhesion or Cohesive Strength of Flame-Sprayed Coatings*, ASTM Designation C633-79. Annual Book of ASTM Standards, Part 17, ASTM, Philadelphia, PA, USA, **1982**, p. 636.
[27] German DIN Standard DIN 50160: *Ermittlung der Haftzugfestigkeit im Stirnversuch*, **1981**.
[28] W. Milewski, *Proc. TS '93*, Aachen **1993**, DVS 152, 258.
[29] C. C. Berndt, *Advances in Thermal Spraying, Proc. ITSC* **1986**, Welding Inst. of Canada, p. 149.
[30] E. A. Ollard, *Trans. Faraday Soc.* **1925**, *21*, 81.
[31] S. Yu. Sharivker, *Poroshk. Metall.* **1967**, *6*(54), 70; *Sov. Powder Met. Metal Ceram.* **1967**, 483.
[32] E. J. Roehl, *Iron Age*, **1940**, *146*, 17, 30.
[33] A. W. Hothersall, C. J. Leadbetter, *J. Electrodepos. Tech. Soc.* **1938**, *14*, 207.
[34] W. Bullough, G. E. Gardam, *J. Electrodepos. Tech. Soc.* **1947**, *22*, 169.
[35] C. Williams, R. A. F. Hammond, *Trans. Inst. Metal Finishing* **1954**, *31*, 124.

[36] Y. M. Rhyim, C. G. Park, S. B. Kim, M. C. Kim, *Proc. 14th ITSC '95*, Kobe, Japan, 22–26 May, **1995**, 773.
[37] H.-D. Steffens, Haftung und Schichtaufbau beim Lichtbogen- und Flammspritzen, Ph.D. Dissertation, Hannover, **1963**.
[38] *Evaluation Methods and Equipment for Flame-Sprayed Coatings*, Metco Inc., Westbury, NY, USA, **1963**, 15 pp.
[39] H. Grützner, H. Weiss, *Surf. Coat. Technol.* **1991**, *45*, 317.
[40] M. Sexsmith, T. Troczynski, *Proc. 14th ISTC '95*, Kobe, Japan, 22–26 May, **1995**, p. 897.
[41] A. Crocombe, R. Adams, *J. Adhes.* **1981**, *12*, 127.
[42] S. Thiele, Mikrohärte, Mikrostruktur und Haftung vakuumplasmagespritzter TiC–Mo_2C–Ni, Co-Verbundschichten, Unpublished Master's thesis, Freiberg University of Mining and Technology, June **1994**, p. 66.
[43] M. Gudge, D. S. Rickerby, R. Kingswell, K. T. Scott, *Proc. 3rd NTSC*, Thermal Spray Research and Applications, Long Beach, CA, USA, 20–25 May, **1990**, p. 331.
[44] E. Lopez, F. Belzung, G. Zembelli, *J. Mater. Sci. Lett.* **1989**, *8*, 346.
[45] E.-H. Meyer, K.-J-Pohl, in: *Moderne Beschichtungsverfahren* (ed. H.-D. Steffens, W. Brandl), DGM Oberursel, **1992**.
[46] M. Müller, Haftungsuntersuchungen an vakuumplasmagespritzten Chromschichten, Unpublished Master's thesis, Freiberg University of Mining and Technology, June **1994**.
[47] Y. Suga, H. Makaba, K. Makabe, Proc. TS'93, Aachen, Germany 1993, DVS 152, 201.
[48] R. B. Heimann, M. Müller, *Proc. 4th Intern. Seminar/Course on Coatings for Aerospace Industry* (CAI-4), Toronto, 26–27 Oct, **1995**; TS'96, Essen, Germany, DVS 175.
[49] D. Lian, Y. Suga, S. Kurihara, *Proc. 14th ISCT '95*, Kobe, Japan, 22–26 May, **1995**, p. 879.
[50] Y. Suga, D. Lian, S. Kurihara, *Proc. 14th ISTC '95*, Kobe, Japan, 22–26 May, **1995**, p. 961.
[51] (a) R. Travis, C. Ginther, C. Zanis, *Advances in Thermal Spraying, Proc. ITSC* **1986**, Welding Inst. of Canada, p. 309; (b) J. W. Maclachlan Spicer, W. D. Kerns, L. C. Aamodt, J. C. Murphy, *Rev. Prog. in Quant. Nondestruct. Eval.* **1990**, *9*, 1169.
[52] G. A. Georgiou, M. B. Saintey, A. M. Lank, D. P. Almond, *Proc. 14th ITSC '95*, Kobe, Japan, 22–26 May, **1995**, p. 1047.
[53] *Standard Test Method for Rockwell Hardness and Rockwell Superficial Hardness of Metallic Materials*, ASTM Designation E18-74. American National Standard Z115.6, ANSI. **1974**.
[54] *Standard Test Method for Microhardness of Materials*, ASTM Designation E384-73. American National Standard Z30.12-1973, ANSI.
[55] J. E. Sundgen, H. T. G. Hentzell, *J. Vac. Sci. Technol. A.* **1986**, *4*, 2259.
[56] P. M. Sargent, T. F. Page, *Proc. Br. Ceram. Soc.* **1978**, *26*, 209.
[57] A. J. Perry, H. K. Pulker, *Thin Solid Films*, **1985**, *124*, 323.
[58] A. J. Perry, E. Horvath, *J. Mater. Sci.* **1978**, *13*, 1303.
[59] E. Horvath, A. J. Perry, *Thin Solid Films* **1980**, *65*, 309.
[60] E. Meyer, *Phys. Z.* **1908**, *9*, 66.
[61] P. J. Burnett, T. P. Page, *J. Mater. Sci.* **1984**, *19*, 845.
[62] A. Thomas, *Surf. Eng.* **1987**, *3*, 117.
[63] P. J. Burnett, D. S. Rickerby, *Thin Solid Films* **1987**, *148*, 41.
[64] E. A. Almond, *Vacuum* **1984**, *35*, 835.
[65] H. Bückle, in: *The Science of Hardness Testing and its Research Applications* (eds. J. W. Westbrook, H. Conrad), ASM, Metals Park, OH, USA, **1971**, p. 453.
[66] B. Jönsson, S. Hogmark, *Thin Solid Films* **1984**, *114*, 257.
[67] J. Lesage, D. Chicot, *Proc. 14th ITSC '95*, Kobe, Japan, 22–26 May, **1995**, p. 951.
[68] A. Iost, J. Aryani-Boufette, J. Foct, *Mém. Et. Sci.: Rev. Mét.* **1992**, *11*, 681.
[69] D. M. Marsh, *Proc. R. Soc. Lond. A* **1964**, *279*, 420.
[70] B. R. Lawn, A. G. Evans, D. B. Marshall, *J. Am. Ceram. Soc.* **1980**, *63*, 574.
[71] L. C. Cox, *Surface Coat. Technol.* **1988**, *36*, 807.
[72] E. Rigal, T. Priem, E. Vray, *Proc. 14th ITSC '95*, Kobe, Japan, 22–26 May, **1995**, p. 851.
[73] E. Lopez, G. Zambelli, A. R. Nicoll, *Proc. TS '90*, Essen **1990**, DVS 130, 241.
[74] J. E. Kelley, J. J. Stiglich Jr., G. L. Sheldon, in: *Surface Modification Technologies* (eds. T. S. Sudarshan, D. G. Bhat), Proc. 1st Int. Conf. Surf. Modification, Phoenix, AZ, USA, 25–28 January, **1988**, The Metallurgical Society, p. 169.

[75] M. O. Borel, R. K. Smith, A. R. Nicoll, *Proc. TS '90*, Essen **1990**, DVS 130, 68.
[76] S. Steinhäuser, B. Wielage, *Proc. 14th ITSC '95*, Kobe, Japan, 22–26 May, **1995**, p. 693.
[77] C. R. Dimond, J. N. Kirk, J. Briggs, *Wear of Materials*, **1983**, *April*, 333.
[78] E. Hornbogen, *Werkstoffe*. Springer Berlin **1991**, p. 202.
[79] *Standard Test Method for Measuring Abrasion Using the Dry Sand/Rubber Wheel Apparatus*, ASTM Designation G65-91, **1991**.
[80] A. W. Ruff, S. M. Wiederhorn, *Treat. Mater. Sci. Technol.* **1983**, *16*, 69.
[81] S. M. Wiederhorn, B. J. Hockey, *J. Mater. Sci.* **1983**, *18*, 766.
[82] I. G. Wright, V. Nagarajan, J. Stringer, *Oxid. Metals* **1986**, *25*(3/4), 175.
[83] W. J. Sumner, J. H. Vogan, R. J. Lindinger, *Proc. Am. Power Conf.* 22–24 April, **1985**, 196.
[84] J. Qureshi, A. Levy, B. Wang, *J. Vac. Sci. Technol.* **1986**, *A4*(6), 2638.
[85] E. R. Buchanan, *Turbomachinery Int.* **1987**, *28*(1), 25–27, 31.
[86] S. T. Wlodek, *EPRI 1885-2, Phase II*, Final Report, **1986**.
[87] A. R. Nicoll, Chapter 13 in: *Coatings and Surface Treatment for Corrosion and Wear Resistance* (eds. K. N. Strafford, P. K. Datta, C. G. Googan), Ellis Horwood, Chichester, UK, **1983**, p. 180.
[88] I. Kvernes, S. Forseth, *Mater. Sci. Eng.* **1987**, *88*, 61.
[89] S. Levine, P. E. Hodge, R. A. Miller, *Proc. 1st Conf. on Advanced Fuel Capable Directly Fired Heat Engines*, Maine Maritime Academy, Castine, ME, USA, 31 July–3 August, 1979; DOE, Washington, DC, USA, **1979**.
[90] N. S. Jacobson, J. L. Smialek, *J. Am. Ceram. Soc.* **1985**, *68*, 432.
[91] G. B. Davies, T. M. Holmes, O. J. Gregory, *Adv. Ceram. Mater.* **1986**, *3*, 542.
[92] M. G. Hebsur, R. V. Miner, *Mater. Sci. Eng.* **1986**, *83*, 239.
[93] M. G. Hebsur, R. V. Miner, *Thin Solid Films*, **1987**, *147*, 143.
[94] J. Gayda, T. P. Gabb, R. V. Miner, *Int. J. Fatigue* **1986**, *8*(4), 217.
[95] C. C. Berndt, *J. Mater. Sci.* **1989**, *24*, 3511.
[96] R. Bauer, Brown, Bovery & Cie, Mannheim, Germany. After [87].
[97] A. R. Nicoll, in: *Coatings for High Temperature Applications*, (Ed. E. Lang), Applied Science Publishers, London, **1983**.
[98] H. Lewis, R. A. Smith, *Proc. 1st Int. Congr. Met. Corr.* **1965**, p. 202. After [87].
[99] S. W. K. Shaw, M. S. Starkey, M. T. Cunningham, High Temparature Corrosion in a Salt Shower Test and Oxidation of a Range of Superalloys, Materials for Gas Turbines: Cost 50, Final Report, March **1979**.
[100] R. Bauer, K. Schneider, H. W. Grünling, *Proc. DOE Conf. on Adv. Mat. for Alternate Fuel Capable Directly Fired Heat Engines*, Castine, ME, USA, **1979**.
[101] A. V. Dean, *Investigation into the Resistance of Various Nickel and Cobalt Base Alloys to Sea Salt Corrosion at Elevated Temparature*, NGTE Report, January **1964**. After [87].
[102] B. Janke, A. R. Nicoll, *Proc. Conf. on Frontiers of High Temperature Materials II*, London, **1983**. After [87].
[103] D. L. Ruckle, *Thin Solid Films*, **1980**, *73*, 455.